https://doi.org/10.5194/egusphere-2025-2669
Preprint. Discussion started: 7 July 2025

High-resolution regional inversion reveals overestimation of anthropogenic methane emissions in China

Shuzhuang Feng[1,2], Fei Jiang[1,2,5*], Yongguang Zhang[1,2], Huilin Chen[3], Honglin Zhuang[1], Shumin Wang[3,4], Shengxi Bai[1], Hengmao Wang[1,2], Weimin Ju[1,2]

[1] *Jiangsu Provincial Key Laboratory of Geographic Information Science and Technology, International Institute for Earth System Science, Nanjing University, Nanjing, 210023, China*

[2] *Jiangsu Center for Collaborative Innovation in Geographical Information Resource Development and Application, Nanjing, 210023, China*

[3] *School of Atmospheric Sciences, Nanjing University, Nanjing, 210023, China*

[4] *Shanxi Province Institute of Meteorological Sciences, Taiyuan 030002, China*

[5] *Frontiers Science Center for Critical Earth Material Cycling, Nanjing University, Nanjing, 210023, China*

[*] Corresponding author: Fei Jiang; Tel.: +86-25-83597077; Fax: +86-25-83592288; E-mail address: jiangf@nju.edu.cn

https://doi.org/10.5194/egusphere-2025-2669
Preprint. Discussion started: 7 July 2025

Abstract

Methane (CH_4), the second most important anthropogenic greenhouse gas, significantly impacts global warming. As the world's largest anthropogenic CH_4 emitter, China faces challenges in accurately estimating its emissions. Top-down methods often suffer from coarse resolution, limited data constraints, and result discrepancies. Here, we developed the Regional Methane Assimilation System (RegGCAS-CH_4) based on the WRF-CMAQ model and the EnKF algorithm. By assimilating extensive TROPOMI column-averaged dry CH_4 mixing ratio (XCH_4) retrievals, we conducted high-resolution nested inversions to quantify daily CH_4 emissions across China and Shanxi Province in 2022. Nationally, posterior CH_4 emissions were 45.1 $TgCH_4 \cdot yr^{-1}$, 36.5% lower than the EDGAR estimates, with the largest reductions in the coal and waste sectors. In North China, emissions decreased most significantly, mainly attributed to the coal and enteric fermentation sectors. Posterior emissions in coal-reliant Shanxi Province decreased by 46.3%. Sporadic emission increases were detected in major coal-producing cities but were missed by the coarse-resolution inversion. Monthly emissions exhibited a winter-low, summer-high pattern, with the rice cultivation and waste sectors showing higher seasonal increases than those in EDGAR. The inversion significantly improved XCH_4 and surface CH_4 concentration simulations, reducing emission uncertainty. Compared to other bottom-up/top-down estimates, our results were the lowest, primarily because the high-resolution inversion better captured local emission hotspots. Sensitivity tests underscored the importance of nested inversions in reducing the influence of boundary condition uncertainties on emission estimates. This study provides robust CH_4 emission estimates for China, crucial for understanding the CH_4 budget and informing climate mitigation strategies.

Keywords CH_4 emissions, Emission inversion, Methane assimilation system, China, Data assimilation

https://doi.org/10.5194/egusphere-2025-2669
Preprint. Discussion started: 7 July 2025

1. Introduction

Methane (CH_4) ranks as the second most significant anthropogenic greenhouse gas and plays a crucial role in global warming. Its global warming potential is 28–29.8 times that of carbon dioxide (CO_2) over a 100-year time scale and contributes approximately 17% to the total radiative forcing of greenhouse gases since the industrial era (Forster et al., 2021; Saunois et al., 2025). With a relatively short steady state atmospheric budget lifetime of slightly over 9 years (Prather, 2007), CH_4 is a key target for rapid climate change mitigation efforts (Tu et al., 2024), as emphasized by the Global Methane Pledge, which aims to reduce global anthropogenic CH_4 emissions by 30% below 2020 levels by 2030 (GMP, 2023). China, as the world's largest CH_4 emitter, accounting for around 14%–22% of global anthropogenic CH_4 emissions, faces a complex challenge (Zhang et al., 2022; Janssens-Maenhout et al., 2019). China's CH_4 emissions originate from diverse sources, with coal mining and rice cultivation being particularly prominent (Nisbet, 2023; Lin et al., 2021). Comprehending the spatiotemporal distribution and trends of China's CH_4 emissions is of utmost importance for formulating effective climate policies and fulfilling international climate commitments.

The bottom-up approaches, which rely on activity data and emission factors, have been widely used to estimate China's CH_4 emissions. However, accurately estimating these emissions remains a significant challenge. Existing inventories are often characterized by large uncertainties in both magnitude and sectoral attribution, with differences between various bottom-up estimates reaching up to 40–60% for China (Saunois et al., 2025). Among the various sources, estimates of China's coal mine CH_4 emissions can range from 14–28 $Tg \cdot yr^{-1}$ (Sheng et al., 2019). This wide disparity leads to much uncertainty in the bottom-up estimates. There are multiple reasons for the uncertainties, especially the lack of comprehensive data on emission sources, especially for small-scale and sporadic emitters, and the use of complex and perhaps inappropriate emission factors in different sectors (Stavert et al., 2022). For instance, in coal mining, the emission factors vary significantly depending on the mining method (underground vs. surface mining), geological conditions, and the quality of coal. More generally, due to the use of a spatial proxy approach for the spatial allocation of the total emissions, existing global inventories exhibit significant spatial discrepancies when compared with high-resolution local measurements, resulting in misattribution of emissions (Qin et al., 2024).

https://doi.org/10.5194/egusphere-2025-2669
Preprint. Discussion started: 7 July 2025

In contrast, top-down inversion methods, that utilize satellite and surface observations in conjunction with atmospheric transport models, have the potential to provide more accurate and comprehensive estimates. Compared with ground-based inversions, satellite-based atmospheric inversions, such as those using column-averaged dry CH_4 mixing ratios (XCH_4) data from the Greenhouse Gases Observing Satellite (GOSAT) or the TROPOspheric Monitoring Instrument (TROPOMI), can offer valuable insights into the spatial distribution of emissions (Lu et al., 2023). Studies utilizing satellite observations have quantified CH_4 emissions from various sources, including oil, gas, and coal mining sectors at the global, regional, and key source scales (Nesser et al., 2024;Bai et al., 2024;Zhang et al., 2021). For instance, Maasakkers et al. (2019) investigated the contribution of different regions to the global CH_4 budget with GOSAT XCH_4 data, identifying areas with significant emissions and sinks. Pandey et al. (2019) used TROPOMI XCH_4 observations to reveal extreme CH_4 leakage from a natural gas well blowout, demonstrating the instrument's ability to detect both large-scale and short-term emission events.

The Methane Emission Control Action Plan released by China explicitly states the exploration and implementation of research on atmospheric methane emission inversion models, and strengthens the verification of emission inventories by inversion data (MECAP, 2023). A number of inversions relevant to China have been conducted with satellite observations. Using inverse analysis of 2019 TROPOMI XCH_4 data, Chen et al. (2022) quantified CH_4 emissions across China and attributed contributions to specific sectors. Zhang et al. (2022) estimated China's CH_4 emissions from 2010 to 2017 by combining satellite and surface observations, revealing complex linkages between emission trends and associated policy drivers. However, the trends of China's CH_4 emissions quantified by the top-down approach (Sheng et al., 2021;Miller et al., 2019) are contrary to those estimated by the bottom-up approach, which is mainly due to the unclear quantification of emissions from the coal mining sector (Sheng et al., 2019;Liu et al., 2021).

Currently, global-scale CH_4 assimilation systems are widely applied, such as CarbonTracker-CH_4 in the United States (Bruhwiler et al., 2014), CAMS in Europe (Agustí-Panareda et al., 2023), NTFVAR in Japan (Wang et al., 2019), LMDz-SACS-CIF in France (Thanwerdas et al., 2022), and GONGGA-CH_4 in China (Zhao et al., 2024). However, significant knowledge gaps remain in accurately estimating CH_4 emissions at the regional scale. There are relatively few existing regional CH_4 assimilation

https://doi.org/10.5194/egusphere-2025-2669
Preprint. Discussion started: 7 July 2025

systems, such as the ICON-ART-CTDAS (Steiner et al., 2024) and CarbonTracker Europe-CH_4 (Tsuruta et al., 2017) in Europe, and the IMI in the United States (Varon et al., 2022). Additionally, existing regional inversions often use global atmospheric transport models with relatively coarse resolutions on the annual or monthly average scale, lacking high-resolution spatial and temporal coverage to capture local characteristics and short-term variations in emissions (Chen et al., 2022). Qu et al. (2021) highlighted significant challenges in separating rice and coal emissions over southeast China due to coarse grid resolution. High-resolution estimates are crucial for understanding the detailed distribution of emissions, especially in regions with heterogeneous source landscapes. For instance, in Shanxi Province, a major coal producing region, the traditional low-resolution models may fail to capture the emissions from numerous small-scale coal mines. Additionally, the inversion results of global and regional systems still show significant differences, mainly due to different observation data, inversion methods, transport models, and resolutions (Kou et al., 2025;Chen et al., 2022;Liang et al., 2023). Another challenge is that regional models need to consider the impact of boundary fields, especially for long-lived species. Current studies usually directly derive regional boundary fields from global simulation or analysis fields, which still contain large errors (Zhang et al., 2022;Kou et al., 2025). Consequently, China's contribution to the global CH_4 budget remains unclear.

In this study, we aimed to address these limitations by developing a Regional Methane Assimilation System (RegGCAS-CH_4) based on the Weather Research and Forecasting-Community Multiscale Air Quality (WRF-CMAQ) model and the Ensemble Kalman Filter (EnKF) algorithm (Evensen, 1994). This system enabled the assimilation of a large volume of TROPOMI XCH_4 data to achieve nested inversions of daily CH_4 emissions with high spatial-temporal resolution. We conducted a comprehensive analysis of the spatial characteristics and monthly variations of China's CH_4 emissions in 2022. In particular, we focused on the nested inversion analysis of CH_4 emissions in Shanxi Province, China.

The novelty of our study lies in the high spatial resolution emission inversions, which allows for capturing the fine-scale features of CH_4 emissions that are often missed by global inversion models. Secondly, by assimilating a larger amount of TROPOMI XCH_4 observations, which feature high spatial resolution, wide spatial coverage, and high-frequency retrievals (~ 100 times more observations than GOSAT) (Qu et al., 2021), we can incorporate the latest and more representative

https://doi.org/10.5194/egusphere-2025-2669
Preprint. Discussion started: 7 July 2025

information on atmospheric CH_4 concentrations to update the daily emissions. This high temporal resolution is essential for understanding the short-term fluctuations in emissions and their response to various factors. Notably, we have pre-updated the global boundary fields, which effectively mitigates the impact of boundary condition errors on regional emission inversions. This is a crucial step that has not been emphasized or implemented in most previous studies. By comparing our results with the currently widely used inventories, we aim to provide a more accurate and detailed understanding of China's CH_4 emissions, which is crucial for formulating effective climate change mitigation strategies.

2. Method and data

2.1 Data assimilation system

The RegGCAS-CH_4 system was extended from RegGCAS (Zhang et al., 2024), which was developed by Feng et al. (2023) based on the Regional multi-Air Pollutant Assimilation System (RAPAS) (Feng et al., 2020) and Global Carbon Assimilation System (GCAS), version 2 (Jiang et al., 2021). RegGCAS-CH_4 includes a regional chemical transport model (CTM) and an ensemble square root filter (EnSRF) assimilation module (Whitaker and Hamill, 2002), which are employed to simulate atmospheric compositions and infer anthropogenic emissions, respectively. The basic framework is almost identical to that in Zhang et al. (2024), in which we inferred the fossil fuel CO_2 emission using surface CO_2 observations. In this study, the system was extended to high-resolution nested inversion for CH_4 emissions, which can optimize emissions from the outer to inner domain and reduce the influence of inaccurate boundary conditions on the inversion of the inner area (Feng et al., 2022). Moreover, the assimilation framework was updated to optimize CH_4 emissions by assimilating the TROPOMI CH_4 column retrievals. The RegGCAS-CH_4 performed a “two-step” inversion scheme in each data assimilation (DA) window. First, the prior emissions were optimized using the available atmospheric observations. Then, the optimized emissions were input back into the CTM to generate the initial fields for the next assimilation window and boundary conditions for the inner domain. Thus, the uncertainties in boundary conditions for the estimates of emissions in the inner domain were also reduced. Simultaneously, the optimized emissions were transferred to the next window to serve as prior emissions. This “two-step” scheme facilitates error propagation and iterative emission optimization, which can ensure the mass conservation of the system and effectively enhance the stability and

https://doi.org/10.5194/egusphere-2025-2669
Preprint. Discussion started: 7 July 2025

consistency of the emission updates (Feng et al., 2024).

2.1.1 Atmospheric transport model

The Weather Research and Forecast (WRF v4.0) model (Skamarock and Klemp, 2008) and the Community Multiscale Air Quality Modeling System (CMAQ v5.0.2) (Byun and Schere, 2006) were applied to simulate meteorological conditions and atmospheric chemistry, respectively. In this study, the CMAQ model employed two-nested simulations. The outer domain (D01), which covered the whole mainland of China with a grid of 225 × 165 cells, and the inner domain (D02), which covered the Shanxi Province and surrounding areas with a grid of 195 × 174 cells, had grid spacings of 27 and 9 km, respectively (Figure 1). There were 20 levels on the sigma–pressure coordinates extending from the surface to 100 Pa. To account for the rapid expansion of urbanization, we updated the underlying surface information for urban and built-up land using the MODIS Land Cover Type Product (MCD12C1) Version 6.1 of 2022. The detailed configuration of WRF-CMAQ is shown in Table S1.

https://doi.org/10.5194/egusphere-2025-2669
Preprint. Discussion started: 7 July 2025

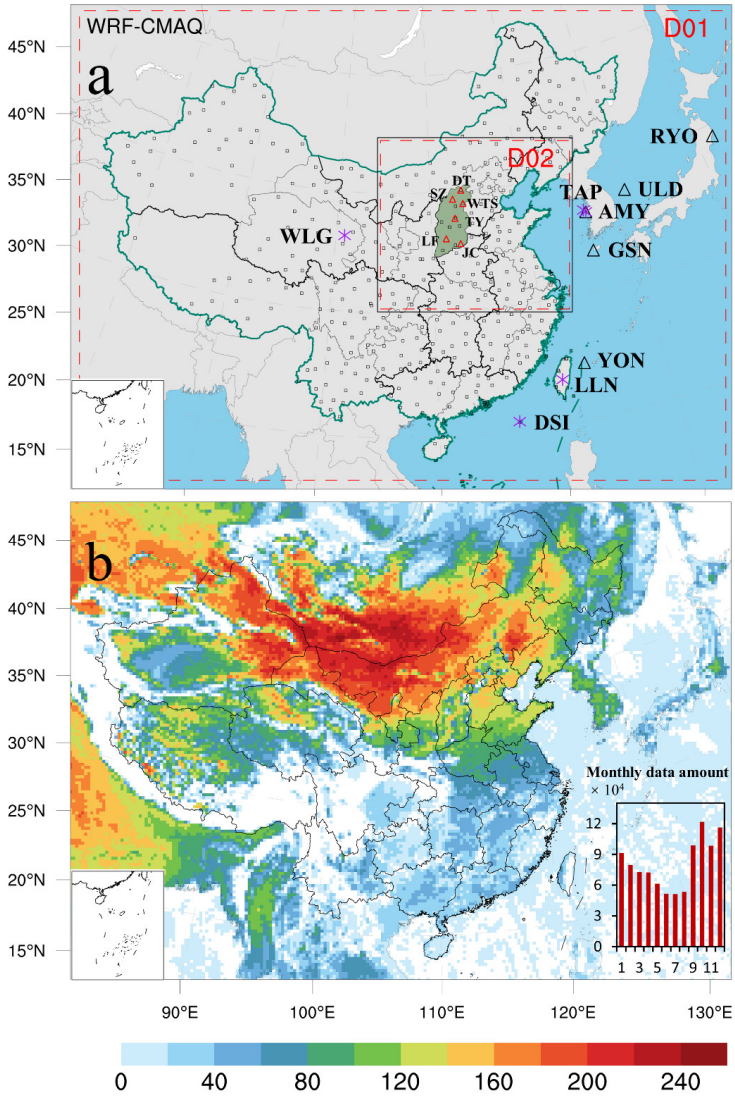

Figure 1 (a) Nested inversion domain and (b) number of TROPOMI XCH_4 retrievals during 2022. The red dashed frame depicts the CMAQ modeling domain; black squares represent the surface meteorological measurement sites; red triangles represent the six *in-situ* CH_4 measurement sites in Shanxi Province; purple asterisks and black triangles represent the flask and *in-situ* CH_4 measurement sites, respectively. The TROPOMI observations that fall within the same model grid are processed and counted as one super-observations. The subfigure in panel (b) shows the total number of super-observations for each month within the study area.

https://doi.org/10.5194/egusphere-2025-2669
Preprint. Discussion started: 7 July 2025

The meteorological initial and lateral boundary conditions were obtained from the Final (FNL) Operational Global Analysis data of the National Center for Environmental Prediction (NCEP) with a 1° × 1° resolution at 6-h intervals. The chemical lateral boundary conditions for the outer domain were derived from the CAMS global inversion-optimized CH_4 concentrations with a 1° × 1° resolution at 6-hour intervals (Bergamaschi et al., 2013), while those for the inner domain were obtained from the forward simulation of the outer domain with optimized CH_4 emissions. In the first DA window, the chemical initial conditions were also extracted from the CAMS, whereas in subsequent windows, they were derived through forward simulation using optimized emissions from the previous window. Since the time required for CH_4 to be transported in the study area is much shorter than its lifetime, to reduce the computational cost to the lowest possible level, we deactivated all the atmospheric chemical reaction processes (Chen et al., 2022; Kou et al., 2025) and incorporated a set of CH_4 tracers variables specifically for conducting ensemble simulations in the CMAQ, enabling all CH_4 concentration sets to be obtained from a single simulation.

It is of utmost importance to eliminate biases in boundary conditions, as any such biases have the potential to cascade through the system. We found that the boundary conditions extracted from the CAMS global fields still had considerable biases over East Asia (see Section 4). Thus, we calculated a scaling factor for each grid of CAMS fields (50°E–160°E, 0°–70°N) against TROPOMI XCH_4 retrievals, and then applied these factors to correct the biases in the boundary conditions of CAMS (Figure S1). Based on each pair of CAMS and TROPOMI data, we first calculated the column concentration of the CAMS reanalysis field. Then, the column concentrations of CAMS and TROPOMI were respectively smoothed in the longitudinal and latitudinal directions with a radius of 4°, and in terms of time using a 4-day window. Subsequently, the latitudinal average values were calculated, along with the average column concentrations biases between CAMS and TROPOMI. After that, linear interpolation was applied to fill in the missing values of the biases in the longitudinal direction. For the biases of the grids where there were missing values at the same latitude, it was assumed that they were consistent with the average biases of the non-missing values at that latitude. Finally, grid-by-grid bias was calculated and correction was carried out for the original CAMS CH_4 concentrations.

https://doi.org/10.5194/egusphere-2025-2669
Preprint. Discussion started: 7 July 2025

2.1.2 EnKF assimilation algorithm

The EnKF is based on the Monte Carlo approach, which uses a stochastic ensemble of model states to approximate the probability distribution of the true state. It has been widely employed for updating the model state by incorporating observational data to minimize the difference between the model-simulated and observed values (Evensen, 1994). The ensemble square root filter (EnSRF) approach, introduced by Whitaker and Hamill (2002), was used to constrain the CH_4 emissions in this study.

The EnSRF process commences with the initialization of an ensemble of model states, which are generated by applying a Gaussian perturbation with an average value of zero and the standard deviation of the uncertainty to a state vector $\boldsymbol{X^b}$. The ensemble-estimated background error covariance matrix $\boldsymbol{P^b}$ is then calculated as:

$$\boldsymbol{P^b} = \frac{1}{N-1}\sum_{i=1}^{N}(\boldsymbol{X_i^b} - \overline{\boldsymbol{X}}^{\boldsymbol{b}})\,(\boldsymbol{X_i^b} - \overline{\boldsymbol{X}}^{\boldsymbol{b}})^T \quad (1)$$

where N is the ensemble size; $\boldsymbol{X_i^b}$ represents the ith sampling; $\overline{\boldsymbol{X}}^{\boldsymbol{b}}$ represents the mean of the ensemble samples. $\boldsymbol{P^b}$ plays a pivotal role in determining how the model state will be adjusted based on new observations.

During the forecast step, each ensemble member is advanced in time using the WRF-CMAQ model. As the model runs, uncertainties in emissions can lead to errors in CH_4 concentrations, and thus the response relationships of the concentration ensembles to the emission ensembles are obtained. In the analysis step, observational data $\boldsymbol{y}$ are incorporated to update the analyzed state. The ensemble mean of the analyzed state $\overline{\boldsymbol{X^a}}$ is regarded as the best estimate of emissions, which is obtained through the following equations:

$$\overline{\boldsymbol{X^a}} = \overline{\boldsymbol{X^b}} + \boldsymbol{K}(\boldsymbol{y} - \boldsymbol{H}\overline{\boldsymbol{X^b}}) \quad (2)$$

$$\boldsymbol{K} = \boldsymbol{P^b H}^T(\boldsymbol{H P^b H}^T + \boldsymbol{R})^{-1} \quad (3)$$

where $\boldsymbol{R}$ is an error covariance matrix; $\boldsymbol{K}$ is the Kalman gain matrix, estimated from the ensemble simulations and determining the relative contributions of observation and background to analysis. The state vector was defined as $\boldsymbol{X^b} = (\boldsymbol{Ea}^T, \boldsymbol{Ep}^T)^T$, where $\boldsymbol{Ea}$ and $\boldsymbol{Ep}$ represent the vectors of CH_4 emissions for the area and power plant sources, respectively. Area sources included the daily total

https://doi.org/10.5194/egusphere-2025-2669
Preprint. Discussion started: 7 July 2025

emissions from the enteric fermentation & manure, landfills & waste, rice cultivation, coal mining, Oil & gas, industry, transport sources, etc. The updated emissions are then used as the new initial states for the next forecast step, creating a cycle of assimilation that gradually refines the estimate of CH_4 emissions.

The observation operator $\boldsymbol{H}$ maps the model state to the observation space. In the context of CH_4, $\boldsymbol{H}$ is configured to first horizontally geo-locate simulated CH_4 concentrations to match the TROPOMI XCH_4 retrievals. Subsequently, it remaps the sub-column concentrations from the 20-layer CMAQ vertical grid to the 12-layer TROPOMI vertical grid by totally or partially allocating CMAQ layers to TROPOMI layers based on pressure edges (Varon et al., 2022). Finally, the column average dry-air mixing ratio $XCH4_s$ can be obtained by applying the TROPOMI column averaging kernel of each layer a_i to sub-columns:

$$XCH4_s = VCH4_s / VAIR_{dry,i} \quad (4)$$

$$VCH4_s = VCH4_p + \sum_{i=1}^{n} a_i \left(XCH4_{s,i} \Delta VAIR_{dry,i} - \Delta VCH4_{p,i}\right) \quad (5)$$

where n is the number of retrieval layers; $\Delta VCH4_{p,i}$ and $VCH4_p$ represent the prior CH_4 column in retrieval layer i and total CH_4 column; $XCH4_{s,i}$ is the simulated dry air mixing ratio of CH_4 in retrieval layer i; $\Delta VAIR_{dry,i}$ and $VAIR_{dry,i}$ represent the dry air column in retrieval layer i and total dry air column, respectively, provided along with the TROPOMI product.

In this study, the DA window was set to 1 d, meaning that daily TROPOMI XCH_4 retrievals were utilized as emission constraints. The ensemble size was set to 50 to fully characterize the system uncertainties and inversion accuracy. To address the problem of spurious long-distance correlations in the EnKF (Houtekamer and Mitchell, 2001), we applied covariance localization using the Gaspari and Cohn function, which is a piecewise continuous fifth-order polynomial approximation of a normal distribution (Miyazaki et al., 2017;Gaspari and Cohn, 1999). Taking into account the transmission distance of CH_4 within one assimilation window, the localization scale was set to 300 km. By setting the covariance to be smaller the farther away from the observations, we could reduce the spurious influence of remote observations on the local analysis.

2.2 Prior emissions and uncertainties

The prior anthropogenic CH_4 emissions were taken from the Emission Database for Global

https://doi.org/10.5194/egusphere-2025-2669
Preprint. Discussion started: 7 July 2025

Atmospheric Research version 8.0 (EDGAR v8), which offers detailed monthly gridded CH_4 emissions at 0.1°×0.1° from various anthropogenic sources (Crippa et al., 2024). The daily emissions, obtained by uniformly allocating the aggregated monthly emission inventory, were directly utilized as the initial estimate in the RegGCAS-CH_4. For natural CH_4 emissions, we utilized the ensemble average of 18 emissions from the WetCHARTs v1.3.1 inventory (0.5◦ × 0.5◦, monthly) in 2019 for wetland emissions (Bloom et al., 2021), the Global Fire Emissions Database (GFED v4.1s, 0.25◦ × 0.25◦, three-hourly) in 2022 for biomass burning emissions (van Wees et al., 2022), and CAMS global emissions inventory (CAMS-GLOB-TERM v1.1, 0.5◦ × 0.5◦, monthly) in 2000 for termite emissions (Jamali et al., 2011). Additionally, CH_4 sinks resulting from soil absorption were derived from datasets simulated by Soil Methanotrophy Model (MeMo v1.0, 1◦ × 1◦, yearly) in 2020 (Murguia-Flores et al., 2018).

Given the model error compensation and the relatively comparable emission uncertainties from one day to the next, we applied an identical uncertainty of 40% to each emission grid at every DA window. Since the RegGCAS-CH_4 adopts a 'two-step' inversion strategy and the daily posterior emissions are iteratively optimized, the emission analysis is generally no longer sensitive to the prior uncertainties of the original emission inventory after several assimilation windows (Zhang et al., 2024).

2.3 Assimilation data and errors

TROPOMI, onboard the Sentinel-5 Precursor satellite, was launched in 2017. Operating in a sun-synchronous orbit with an equator local overpass time of 13:30 h, TROPOMI offers daily global continuous monitoring of XCH_4. The RemoTeC full-physics algorithm is used to retrieve XCH_4 from TROPOMI measurements of sunlight backscattered by Earth's surface and atmosphere in the near-infrared (NIR) and shortwave-infrared (SWIR) spectral bands (Lorente et al., 2022). After 2019, the spatial resolution of TROPOMI was adjusted to a remarkable 5.5×3.5 km^2 at nadir, enabling the identification of even relatively small-scale CH_4 emission sources. We used the TROPOMI XCH_4 level 2 data product to estimate CH_4 emissions.

All TROPOMI individual pixels with a quality assurance value (qa_value) smaller than 0.5 were discarded, which corresponds to high-cloud conditions or the presence of snow or ice. However, we still found many unrealistic low values, especially in summer. To further minimize the impact of outliers, we selected another XCH_4 product generated based on the WFMD algorithm for cross-

https://doi.org/10.5194/egusphere-2025-2669
Preprint. Discussion started: 7 July 2025

validation (Schneising et al., 2023). Only those pixels that were concurrently available in the TROPOMI/WFMD product and met the quality flag requirements were assimilated. Figure 1b illustrates the observational amount of TROPOMI XCH_4 in 2022 at each grid. Although the distribution of filtered data exhibits spatial nonuniformity, most grid cells in the central-northern regions with intense anthropogenic emissions have observational coverage for more than 100 days in 2022. Additionally, the monthly variation in the data amount shows fluctuations, with the peak occurring at the beginning and end of the year and the troughs around the middle. According to the latest quarterly validation report, the 1σ spread of the relative difference between the TROPOMI and the TCCON (Wunch et al., 2011) is of the order of 0.7% for bias corrected product, which is recommended to be considered as an upper boundary of the random uncertainty of the satellite data (Lambert et al., 2024).

2.4 Evaluation Data

To evaluate the performance of the WRF simulations, we utilized the surface meteorological measurements of 400 stations with 3-hour intervals, including temperature at 2 m (T2), relative humidity at 2 m (RH2), and wind speed at 10 m (WS10). These measurements were obtained from the National Climate Data Center (NCDC) integrated surface database (http://www.ncdc.noaa.gov/oa/ncdc.html, last access: 25 August 2024). Overall, the WRF demonstrated satisfactory performance in reproducing meteorological conditions over China (Figure S2), with minimal biases of -0.4°C for T2, -4.9% for RH2, and 0.5 m/s for WS10, respectively. To evaluate the posterior CH_4 emissions, two parallel forward modeling experiments were conducted: the control experiment with prior emissions (CEP) and the validation experiment with posterior emissions (VEP). Both experiments utilized identical meteorological fields, as well as initial and boundary conditions. We evaluated: (1) the simulated XCH_4 against TROPOMI XCH_4; (2) the simulated surface CH_4 concentrations against independent ground CH_4 observations from eleven *in-situ* and five flask monitoring sites (Table S2). The *in-situ* measurements included five global sites outside China (AMY, GSN, RYO, ULD, and YON) with hourly resolution from NOAA's GLOBALVIEWplus CH_4 ObsPack v6.0 (Schuldt et al., 2023), as well as six regional sites in Shanxi Province (TY, DT, LF, SZ, JC, and WTS) equipped with Picarro G2301 analyzers for high-precision, 5-second CH_4 measurements (data were processed as daily averages to reduce random errors). The Picarro instrument, based on

https://doi.org/10.5194/egusphere-2025-2669
Preprint. Discussion started: 7 July 2025

wavelength-scanned cavity ring-down spectroscopy technology, is designated by the World Meteorological Organization as the international reference instrument for CH_4 observations in international comparisons. Additionally, observations from five flask sampling sites (AMY, DSI, LLN, TAP, and WLG) were also obtained from ObsPack dataset, providing weekly measurements.

3. Results and discussion

3.1 Posterior CH_4 emissions

Figure 2 shows the spatial distributions of the estimated annual CH_4 emissions and the differences from the prior emissions (i.e., EDGAR) over China in 2022. On a national scale, the high CH_4 emissions were primarily concentrated in the Yangtze River Delta (YRD), Pearl River Delta (PRD), North China Plain (NCP), and Shanxi Province. For the YRD and PRD characterized by high-density populations, a large number of industrial plants, as well as extensive agricultural activities such as rice cultivation, contributed significantly to CH_4 emissions. The NCP, with its heavy reliance on coal-based energy and large-scale livestock farming, was also expected to be a major emission source. Lower emissions were mainly distributed across Northwest, and Southwest China.

Compared with the EDGAR, the posterior emissions were generally smaller over most areas of mainland China, with total anthropogenic emissions decreasing to 45.1 $TgCH_4 \cdot yr^{-1}$, 36.5% lower than the EDGAR (71.0 $TgCH_4 \cdot yr^{-1}$). Additionally, previous studies have consistently shown that the EDGAR inventory overestimates China's CH_4 emissions. For example, through a Bayesian inversion of CH_4 and stable isotope ($\delta^{13}C$-CH_4) measurements for East Asia, Thompson et al. (2015) found that posterior values decreased significantly across eastern and southern China, especially in the NCP. Overall, EDGAR overestimated China's emissions by 29%. Similarly, Zhang et al. (2021) conducted a global inverse analysis using GOSAT observations and revealed that EDGAR significantly overestimates anthropogenic emissions in eastern China. The posterior estimate of Chinese anthropogenic emissions was 30 % lower than that of EDGAR. Turner et al. (2015) also demonstrated that after assimilating GOSAT observations, China's posterior CH_4 emissions were revised downward by 50% relative to EDGAR. Using a regional model to assimilate TROPOMI observations, Kou et al. (2025) detected decreases of varying magnitudes across nearly the entirety of China, with the exception of Northwest China. Similar results have been reported by Alexe et al. (2015), Pandey et al. (2016),

https://doi.org/10.5194/egusphere-2025-2669
Preprint. Discussion started: 7 July 2025

and Maasakkers et al. (2019). Our study, using a higher-resolution regional inversion method, provided more detailed emission information. Overall, our inversion results were comparable to the ensemble mean of GCP ground-based inversions (Wang et al., 2025).

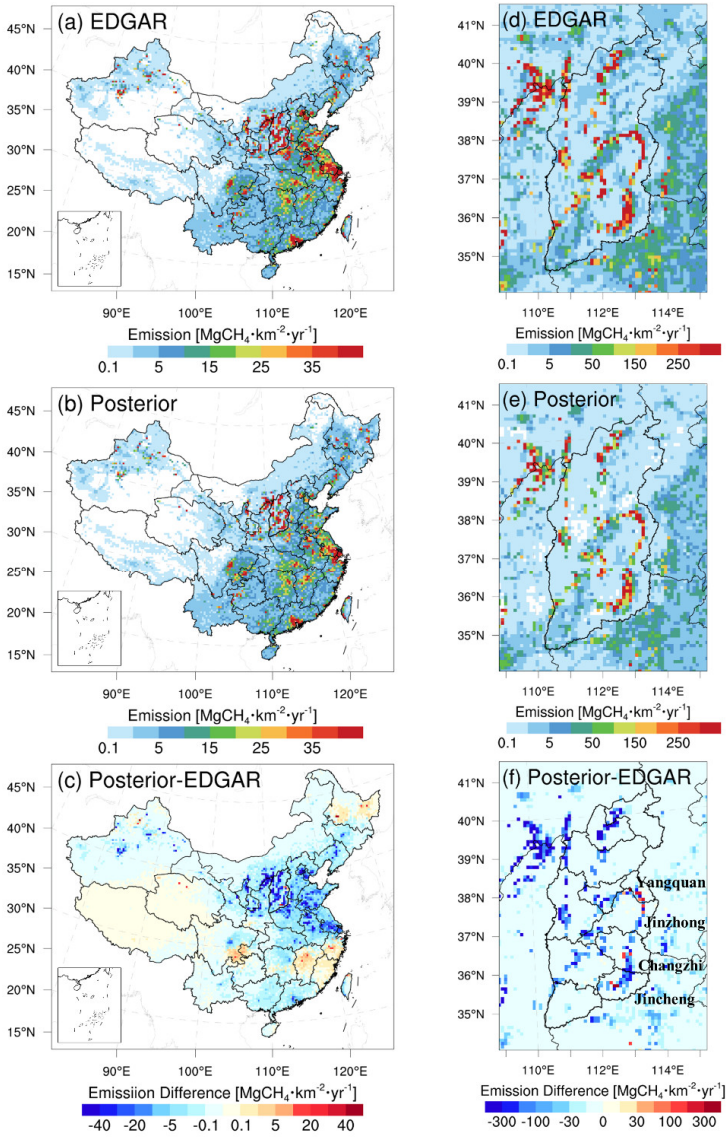

Figure 2 Spatial distribution of the annual total prior emissions (top, EDGAR v8, $MgCH_4 \cdot km^{-2} \cdot yr^{-1}$), posterior emissions (middle), and differences (borrom, posterior minus prior) over (a-c) Mainland China and (d-f) Shanxi Province.

https://doi.org/10.5194/egusphere-2025-2669
Preprint. Discussion started: 7 July 2025

Table 1 shows the comparison of posterior and prior anthropogenic CH_4 emissions of the main emission sectors in China. Consistent with the previous studies, we also found that North China is the region with the most significant reduction nationwide. Almost the entire region has experienced a decrease, with a reduction of 56.9%, indicating that there are indeed substantial systematic biases in the EDGAR inventory. Among them, the coal sector contributed the most to this discrepancy, followed by enteric fermentation, with decreases of 56.2% and 64.0%, respectively (Table 1).

For Northeast China, the increase in emissions mainly occurred in Heilongjiang Province, especially in the western part, which is the base of Daqing Oilfield, China's largest oilfield. The oil and gas sectors in the entire Northeast China increased by 27.1% and 23.1%, respectively. However, emissions from other sectors decreased, resulting in an overall 11.1% reduction in emissions. Rice paddy CH_4 emissions serve as the dominant emission source in East China. However, the high spatial heterogeneity and the insufficiency of data on rice cultivation introduce large uncertainties to inventories. Additionally, different fertilization management practices in various regions, such as the use of nitrogen fertilizer versus organic fertilizer (Zhang et al., 2022), and mid-season drainage management (Lin et al., 2021), bring about considerable uncertainties in the emission factors related to rice cultivation practices. Emissions in Zhejiang, Fujian, and Jiangxi Provinces increased, mainly attributed to emissions from rice paddies. In contrast, emissions in other provinces decreased, dominated by the coal mining, leading to an overall 26.4% reduction in emissions in East China. In Central and South China, the dominant sources of emissions remain rice paddies. However, the decreases were mainly attributed to the coal mining and wastewater treatment sectors, which reduced emissions by 51.3% and 12.4%, respectively. Overall, the total emissions in these two regions decreased by 21.8% and 7.8%, respectively. In Northwest China, the reduction in emissions was mainly distributed in the hotspot areas of coal mines, which dominated the overall 55.7% decrease in emissions. In Southwest China, the increase in emissions occurred predominantly in the southern part of the Sichuan Basin, a major coal-producing region, while emissions in other regions decreased. Sheng et al. (2019) found that the EDGAR inventory lacks a significant amount of statistics on coal mines. Moreover, China has issued an energy policy of “phasing out small coal mines” (approximately 50% of which are located in the southwest with high CH_4 content) to shift production towards lower-emission areas and consolidate into large coal mines (Zhang et al., 2022;Sheng et al., 2019).

https://doi.org/10.5194/egusphere-2025-2669
Preprint. Discussion started: 7 July 2025

Additionally, the wastewater treatment sector achieved significant emission reductions, driving a 1.7% overall decrease in Southwest China.

Table 1 Comparison of posterior and prior anthropogenic CH_4 emissions ($GgCH_4 \cdot yr^{-1}$) of the main emission sectors in the 7 major regions of China. Waste includes wastewater treatment, solid waste landfills, and solid waste incineration.

		Coal	Gas	Rice	Waste	Livestock	Building	Mature
North	Prior	13841.1	98.4	169.1	2462.1	3882.9	385.5	859.5
	Posterior	6068.4	46.2	116.4	1238.1	1396.4	206.7	279.6
Northeast	Prior	771.9	82.6	879.6	1427.9	251.9	268.4	36.8
	Posterior	665.0	101.8	821.2	1259.6	237.7	243.3	34.1
East	Prior	2257.3	54.4	5100.3	6681.4	907.9	732.9	200.5
	Posterior	1114.5	45.1	4592.4	4750.9	512.7	576.2	114.4
Central	Prior	846.5	32.4	3139.5	1882.9	434.2	399.4	91.2
	Posterior	412.2	25.7	2862.6	1324.4	343.3	314.1	75.2
South	Prior	15.0	20.5	2186.4	1622.5	280.2	254.6	44.0
	Posterior	13.8	18.9	2080.6	1421.3	269.9	235.0	42.2
Northwest	Prior	8188.3	1083.4	143.3	970.5	746.2	226.7	76.4
	Posterior	2899.1	645.8	120.7	593.6	534.3	164.4	39.6
Southwest	Prior	531.3	76.5	2046.4	1124.0	667.0	356.3	107.1
	Posterior	505.6	77.2	2063.0	1060.7	663.7	352.1	107.2

China accounts for as high as 69% of the global mitigation potential in coal mining in 2030 (EPA, 2019). Shanxi Province, where 94% of the emissions come from the coal mining sector, counts for nearly one-third of the country's total CH_4 emissions. Therefore, we conducted a focused analysis on the emissions in Shanxi Province with high-resolution (9 km) inversion, which can better diagnose the spatial characteristics of emissions caused by coal mining (Figure 2d-f). The optimized emissions showed a decrease in the vast majority of areas in Shanxi Province. Compared with the EDGAR inventory (9.0 $TgCH_4 \cdot yr^{-1}$), the posterior emissions decreased by 46.3% to 4.8 $TgCH_4 \cdot yr^{-1}$. The overestimation of coal mining emissions may be due to the fact that the standard IPCC emission factors used by EDGAR are too high for Chinese coal mines (Lin et al., 2021). Additionally, the average

https://doi.org/10.5194/egusphere-2025-2669
Preprint. Discussion started: 7 July 2025

emission factors in the north are lower than those in other regions (Gao et al., 2021). The use of a uniform regional emission factor by EDGAR further exacerbates the overestimation of emissions (Shi et al., 2025). Moreover, in the past decade, the extraction and utilization of coal mine CH_4 in China have been largely improved (Lu et al., 2021), but the recovery of coal mine CH_4 is not adequately considered in the EDGAR inventory. Finally, the CH_4 emission intensity of surface mining is ten times lower than that of underground mining. However, surface mining is overlooked in the EDGAR inventory (Gao et al., 2020). In Yangquan, Jincheng, Changzhi, and Jinzhong cities (Figure 2), some increased emission hotspots caused by the coal mining activities could be found. Coincidentally, these cities are the main coal-producing areas in Shanxi Province. Overall, the emissions in these cities have still decreased by 3.3%, 4.2%, 29.5%, and 32.3%, respectively (Figure S3). Tu et al. (2024) utilized TROPOMI observations and implemented a wind-assigned anomaly method to quantify the CH_4 emissions from coal mines in Yangquan, Changzhi, and Jincheng. Compared to EDGAR, emissions decreased by 56.5%, 40.5%, and 65.0%, respectively—a larger reduction than our findings.

3.2 Monthly variations

Figure 3 illustrates the comparison of the monthly variations in prior and posterior emissions both in China and Shanxi province. Nationally, influenced by CH_4 emissions from paddy fields, both the prior and posterior emissions exhibited the characteristic of being low in winter and high in summer. However, the posterior emissions for each month were lower than the prior emissions. The monthly posterior emissions ranged from 2.3 to 7.5 $Tg \cdot month^{-1}$, with a modification rate ranging from -30.7% to 5.6% compared to the prior emissions (4.8–7.6 $Tg \cdot month^{-1}$). The month with the smallest difference occurred in August, mainly because the underestimation of CH_4 emissions from paddy fields compensated for the overestimation of emissions from coal mining (Figure 3c). Additionally, due to the weather conditions such as clouds and rain in summer, the amount of TROPOMI data was significantly smaller than that in other seasons (Figure 1b), which might lead to insufficient constraints on emissions. Regarding Shanxi Province, even with an agnostic flat monthly prior (Figure 3b), our estimates generated a monthly variation, and emissions in all months were lower than the prior values. We also detected a decrease and subsequent increase in emissions that correspond to the Spring Festival in February. A noticeable recovery of production capacity in the following two months was also evident. Overall, although relatively large uncertainties were introduced by the amount of

https://doi.org/10.5194/egusphere-2025-2669
Preprint. Discussion started: 7 July 2025

observations, the seasonal variation of monthly posterior emissions could be roughly captured.

To gain a deeper understanding of the posterior emissions, the assimilated estimations were allocated to different emission sectors, based on the monthly prior proportions at the model grid points. The sectoral patterns offer insights into the underlying factors influencing China's emission changes. Consequently, we further concentrated on interpreting the emissions from the coal, gas, rice cultivation, waste, livestock, building, and manure management sectors, which are the most significant sectors in China (Table S3).

It could be found that the reduction in emissions each month in China was mainly dominated by the coal sector, with an overall annual reduction of 55.9%, indicating a high level of uncertainty in the prior emissions. Moreover, the gas, livestock, and manure management sectors also showed varying degrees of reduction in different months, with overall decreases of 34.0%, 45.1%, and 51.5%, respectively. However, for the rice cultivation sector, the posterior emissions were lower than the prior emissions in the first half of the year, while the situation was reversed in the second half of the year. Summer and autumn are the heading and flowering stages for both single-cropping late rice and double-cropping late rice across the eastern, central, and southern China. During these periods, the emissions from paddy fields tended to be higher than in other seasons. Overall, the posterior CH_4 emissions from paddy fields have slightly decreased by 4.7%. A similar situation was observed in the waste sector. Previous studies have shown that significant CH_4 production in wastewater is more likely to occur because methanogens become more active as the temperature rises (Hu et al., 2023). Therefore, a significant increase in the posterior emissions compared to the prior emissions could be observed in August. For the building sector, due to winter heating or hot water supply, the emissions in winter were approximately three times higher than those in summer. After optimization, the emissions in winter and spring significantly decreased, while in some months of summer and autumn, the decrease was less pronounced, and there was even a slight increase. The inter-monthly difference in emissions decreased, but the monthly variation remained significant. Overall, the posterior emissions have decreased by 25.4%. The changes in emissions in Shanxi Province were mainly dominated by the coal mining sector. Compared to EDGAR, the monthly reduction rate ranged from 12.6% in August to 67.3% in February. For other sectors, there was little overall monthly variation.

https://doi.org/10.5194/egusphere-2025-2669
Preprint. Discussion started: 7 July 2025

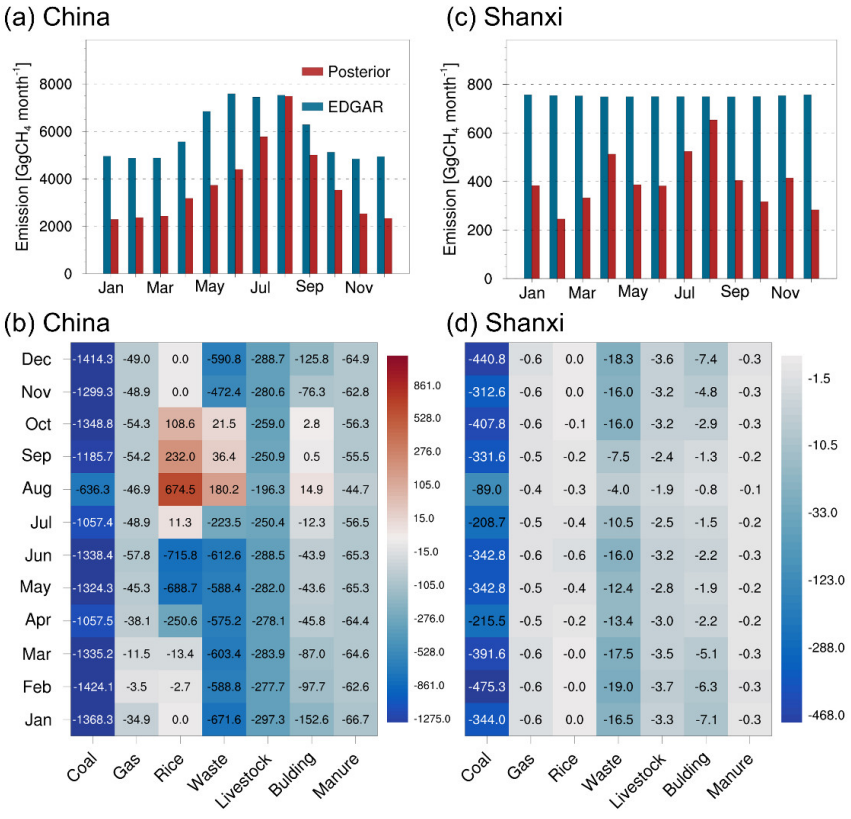

Figure 3 Comparison of the monthly variations and the sectoral differences ($GgCH_4 \cdot mon^{-1}$) in prior and posterior CH_4 emissions over (a, b) China and (c, d) Shanxi Province.

3.3 Evaluation of posterior emission estimates

Figure 4 shows the spatial distribution of XCH_4 in the posterior simulation, as well as the validation of XCH_4 simulated by prior and posterior emissions with TROPOMI observations. It could be observed that relatively large XCH_4 were present over eastern China, which was driven by coal mining in the northern part and rice paddy fields in the southern part (Zhang et al., 2023). The simulation using prior emissions significantly overestimated the XCH_4 concentration in China, especially in the NCP. The maximum overestimation exceeded 100 ppb, which was consistent with the overestimated emissions in these regions (Figure 2). After the inversion optimization, the simulated XCH_4 showed better spatial distribution consistency with the TROPOMI observations. The vast majority of the biases were within 20 ppb, and the national average biases decreased from 14.7 ppb to 7.9 ppb, representing

https://doi.org/10.5194/egusphere-2025-2669
Preprint. Discussion started: 7 July 2025

a 46.0% reduction. In Shanxi Province, high emissions were mainly concentrated in the coal-rich southeastern region, with an annual average maximum exceeding 1970 ppb, which was difficult to reproduce the characteristics of local high concentrations at a coarse resolution. The prior simulation showed obvious overestimation across the entire region, particularly in northern Shanxi. Due to the high spatial resolution adopted, the model could take into account more practical factors, and thus capture the spatiotemporal variations of emission sources and transport processes more precisely. As a result, the agreement between the posterior simulations and the TROPOMI observations was remarkably enhanced. The average deviation decreased from 37.9 ppb to 11.9 ppb, with a reduction of 68.7%. These changes not only demonstrate the effectiveness of reducing uncertainties in optimizing emission sources but also imply that there are indeed significant uncertainties in the prior emission inventory.

https://doi.org/10.5194/egusphere-2025-2669
Preprint. Discussion started: 7 July 2025

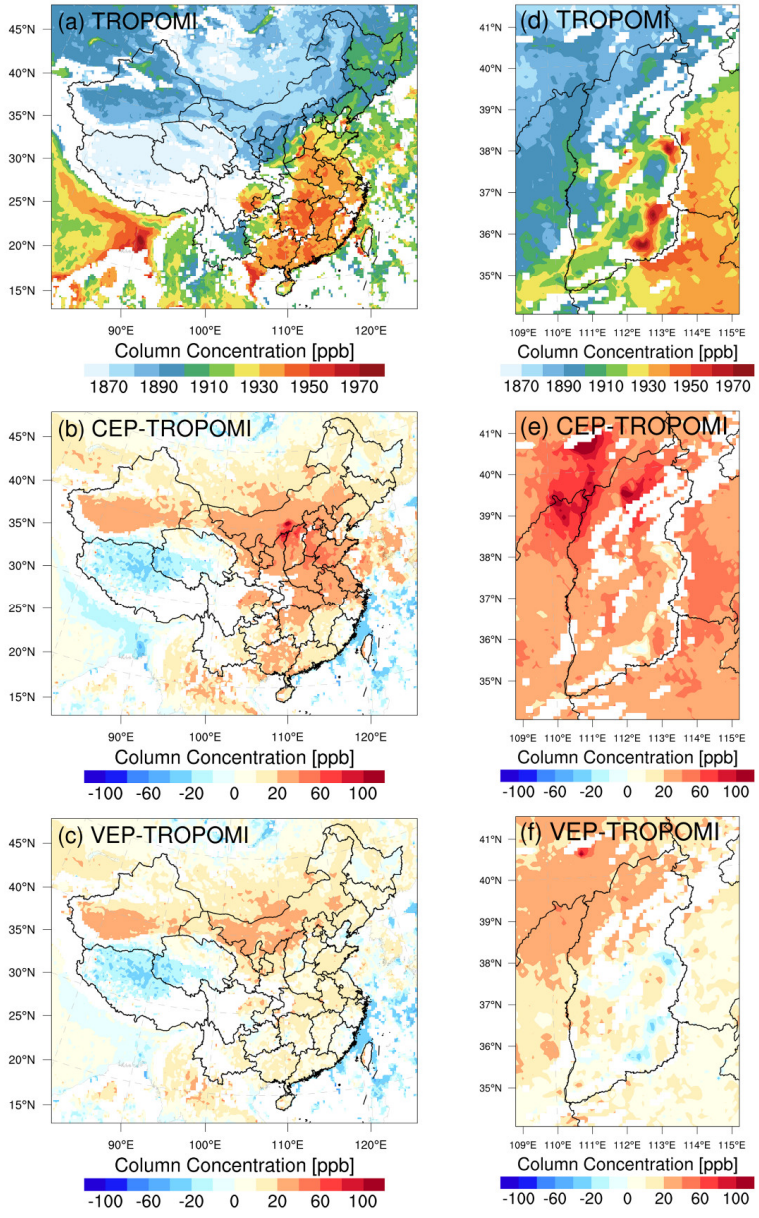

Figure 4 Comparison of simulated XCH_4 (ppb) from prior and posterior emissions with TROPOMI observations over (a-c) China and (d-f) Shanxi Province. (a, d) Spatial distribution of XCH_4 observed by TROPOMI. (b, e) Differences between prior simulations and observations. (c, f) Differences between posterior simulations and observations.

https://doi.org/10.5194/egusphere-2025-2669
Preprint. Discussion started: 7 July 2025

We further conducted an independent evaluation of the posterior estimate by comparing it with 10 *in-situ* and flask monitoring sites from the CH_4 ObsPack v6.0 database. Figure 5 shows the time series comparison of the CEP and VEP experiments with the observations. The evaluation statistics for all sites are presented in Table S4. There was a significant overestimation in the CEP experiment throughout most of the study period. Although most of the sites are located in the eastern regions outside China, influenced by the atmospheric circulation, the westerlies prevail in most parts of China. Thus, the optimized emission information can be effectively reflected in the concentrations observed downwind. The optimized simulation in VEP experiments was more consistent with the observations. Among them, the AMY flask site showed the largest reduction in bias, with the average bias decreasing from 35.3 ppb to 3.3 ppb, a decrease of 90.7%. For WLG, the only ObsPack site available in mainland China, the average bias decreased from 47.4 ppb to 28.3 ppb, a reduction of 40.3%. This indicates that the optimized emissions can significantly improve the CH_4 simulation, whether in areas close to the source or downwind of the source. Overall, the average bias of the 10 sites decreased by 58.6%, from 28.6 ppb to 11.9 ppb, the root mean square error (RMSE) decreased by 28.9%, from 56.2 ppb to 39.9 ppb, and the correlation coefficient (CORR) increased from 0.72 to 0.75. These evaluation results demonstrate that the inversion effectively reduces the uncertainties of prior emission inventory.

https://doi.org/10.5194/egusphere-2025-2669
Preprint. Discussion started: 7 July 2025

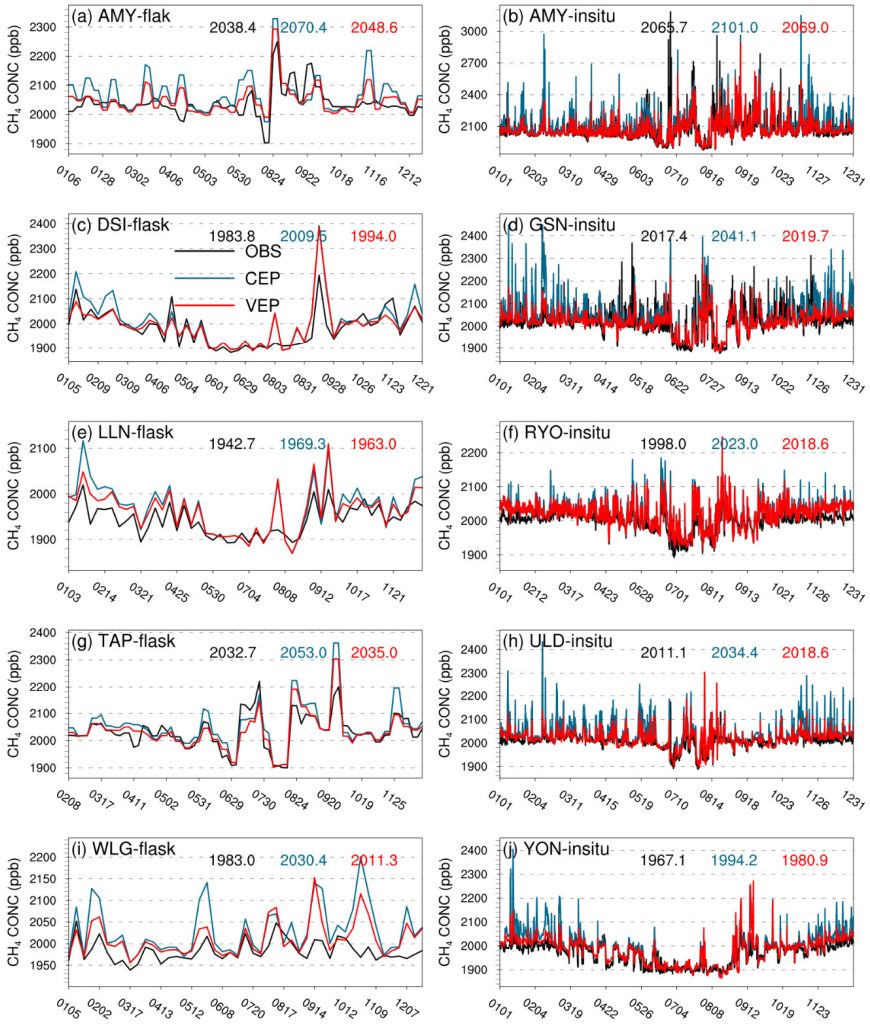

Figure 5 Time series comparison of surface CH_4 concentrations (ppb) from prior (CEP) and posterior (VEP) emission simulations with observations from 5 flask sites and 5 *in-situ* sites within the ObsPack dataset. The black, blue, and red values represent the averaged observations, prior simulations, and posterior simulations, respectively.

We also carried out an independent validation using six high-precision *in-situ* observation sites within Shanxi Province (Figure 1a). Table 2 shows the bias, RMSE, and CORR of the CEP and VEP simulations against these surface observations. Except for the LF site, where the VEP experiment exhibited an underestimation, the VEP experiment demonstrated varying degrees of improvement at

https://doi.org/10.5194/egusphere-2025-2669
Preprint. Discussion started: 7 July 2025

the other five sites. Notably, the bias reduction at the DT and WTS sites exceeded 93.3%. Especially for the WTS site, a high mountain site with an altitude of over 2208 m, the bias was decreased to 8.3 ppb. On average across all sites, the bias significantly decreased by 96.0%, from 535.1 ppb to 21.4 ppb. For the RMSE, the most significant decreases were observed at the DT and SZ sites, both exceeding 73%. Overall, the RMSE reduction ranged from 13.5% to 79.0%. Additionally, the CORR of the VEP experiment increased to 0.48–0.63. In addition, we evaluated the CH_4 concentration simulation for the afternoon, during which the model generally demonstrates better boundary layer simulation performance, with overall lower bias and higher CORR (Table S5). These results further confirm that the RegGCAS-CH_4 system can effectively capture the characteristics of high-resolution CH_4 emission changes and improve the accuracy of concentration simulations.

Table 2 Statistics comparing the daily average CH_4 concentrations (ppb) from the simulations with prior (CEP) and posterior (VEP) emissions against six independent surface *in-situ* observation sites in Shanxi Province, respectively. The numbers under the site names represent the number of valid observations.

Site Name	Mean Obs.	Mean Sim.		BIAS		RMSE		CORR	
		CEP	VEP	CEP	VEP	CEP	VEP	CEP	VEP
TY (351)	2595.5	2771.0	2353.2	175.4	-242.3	408.7	353.6	0.46	0.51
DT (286)	2122.0	2441.1	2139.2	319.1	17.2	489.0	102.6	0.49	0.58
LF (277)	2395.1	2397.2	2197.9	2.0	-197.3	186.8	257.3	0.45	0.35
SZ (359)	2148.8	4560.5	2782.4	2411.7	633.6	2778.1	745.1	0.44	0.48
JC (362)	2446.0	2624.5	2355.2	178.4	-90.9	385.0	356.3	0.52	0.52
WTS (361)	2064.0	2188.0	2072.2	124.1	8.3	162.6	59.1	0.49	0.63

* BIAS, mean bias; RMSE, root mean square error; CORR, correlation coefficient

4. Discussion

To further explore the characteristics of our posterior emissions and offer valuable guidance for the

https://doi.org/10.5194/egusphere-2025-2669
Preprint. Discussion started: 7 July 2025

refinement of bottom-up inventory in China, we conducted a comparison analysis with the latest 8 bottom-up inventories and 4 top-down emission estimates (Figure 6). Specifically, apart from EDGAR v8, the bottom-up inventories were sourced from the Copernicus Atmosphere Monitoring Service (CAMS v6.2) (Soulie et al., 2024), Community Emissions Data System (CEDS_202407) (Hoesly et al., 2018), Evaluating the Climate and Air Quality Impacts of Short-Lived Pollutants inventory (ECLIPSE v6b) from the GAINS model (Stohl et al., 2015), Global Carbon Project (GCP 2024) (Saunois et al., 2025), Peking University (PKU v2) (Liu et al., 2021), United Nations Framework Convention on Climate Change (UNFCCC, 2020), and the United States Environmental Protection Agency (EPA, 2019). In addition, we also obtained the Global Fuel Exploitation Inventory (GFEI v2) (Scarpelli et al., 2022) to assess the emissions from the coal mining sector in Shanxi Province. The top-down emissions were mainly sourced from the CarbonTracker-CH_4 (Oh et al., 2023) and the research results of Chen et al. (2022), Kou et al. (2025), and Peng et al. (2023).

Typically, the top-down estimates showed lower emissions than the bottom-up inventories. Although our posterior estimates were the lowest across all datasets, they closely matched CEDS, PKU, and CarbonTracker-CH_4 and comparable to the ensemble mean of GCP ground-based inversions (Wang et al., 2025). Overall, our posterior emissions were 22.0% lower than the average of bottom-up inventories and 16.6% lower than the previous top-down estimates. The lower emissions in this study were predominantly driven by the downward revision of coal emissions. Overestimated emission factors and the difficulty in tracking the spatial distribution of coal mines due to mine closures and regional transfers remain significant obstacles to the assessment of coal mine emissions (Gao et al., 2021). Our estimate was lower than the previous top-down studies (53–65 Tg yr^{-1}), likely because those previous studies were conducted at much coarser resolutions (0.3°–2.5° versus 27 km) or with much sparser observations (*in-situ* ground measurements and GOSAT versus TROPOMI). For Shanxi Province, compared with the bottom-up inventories, our results were close to those of GAINS and fell within the uncertainty range of Qin et al. (2024), which set multiple groups of emission factors according to coal types, mining methods, and geological structures. There were substantial disparities among the top-down inversions. Notably, for CarbonTracker-CH_4, despite having minimal divergence at the national scale when contrasted with other estimations, the values for Shanxi Province were markedly lower than those of other estimates. This could be attributed to the insufficient assimilation

https://doi.org/10.5194/egusphere-2025-2669
Preprint. Discussion started: 7 July 2025

of China's surface observations and systematic biases in the spatial distribution of prior emissions. Overall, the coal-mining emissions in this study were 29.2% lower than the bottom-up inventories and 19.3% lower than the previous top-down inversions.

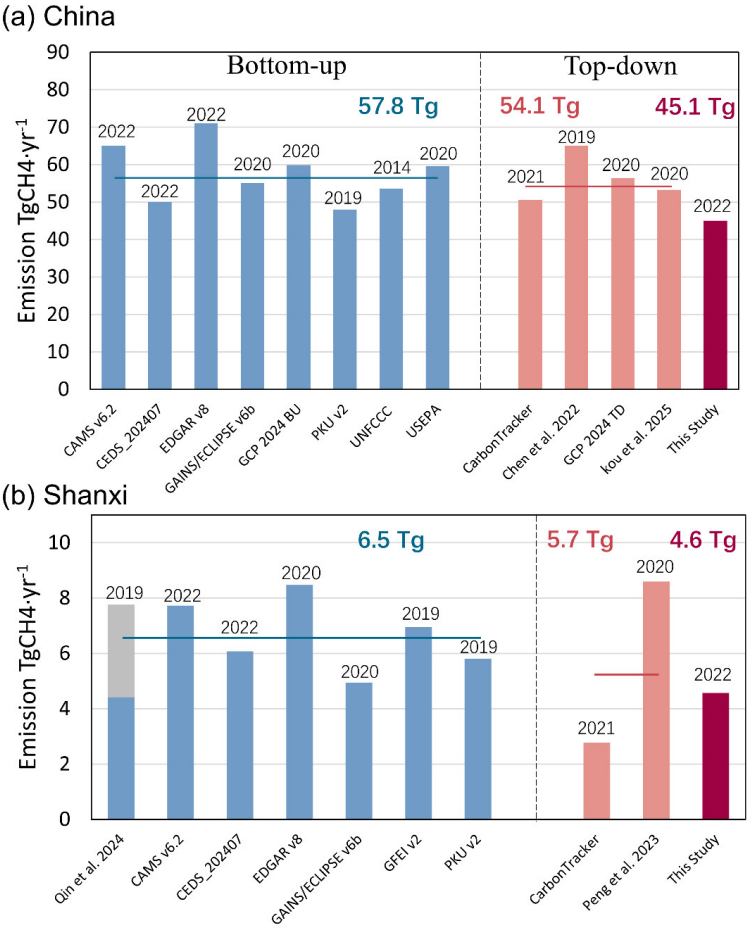

Figure 6 Total anthropogenic CH_4 emissions ($TgCH_4 \cdot yr^{-1}$) in China (a) and CH_4 emissions from the coal mining sector in Shanxi Province (b). GCP 2024 BU and GCP 2024 TD represent the bottom-up and top-down ensemble means included in the dataset, respectively. The grey bars in panel b represent the range of CH_4 emissions estimated by Qin et al. (2024) using four different methods. The latest year in the inventory is marked above the bars.

Uncertainties in boundary conditions constitute a significant source of error in regional inversion. Despite the optimization of concentration fields in the CAMS, significant biases remained evident

https://doi.org/10.5194/egusphere-2025-2669
Preprint. Discussion started: 7 July 2025

(Figure 7a). To address this issue, we implemented additional constraints on the CAMS concentration fields using TROPOMI XCH_4 observations, resulting in a notably improved agreement with the observations. Specifically, the average bias decreased from -3.7 ppb to -1.0 ppb, representing a reduction of 73.7%. A sensitivity experiment (SENS) was further conducted, where the unadjusted CAMS global fields were extracted as boundary conditions to invert anthropogenic CH_4 emissions, aiming to evaluate the impact of boundary condition uncertainties on regional emission inversions. Compared with the base experiment (BASE), the largest discrepancies in monthly variations were observed during the winter months, indicating significant overestimations. The emission differences across different months closely aligned with the concentration differences, suggesting that underestimations in concentrations prompted more substantial emission adjustments for compensation. Regarding the spatial distribution, due to the relative long lifetime of CH_4, emission changes caused by boundary condition biases were not confined to regional boundaries, such as in Northeast and Northwest China, but were also observable throughout the entire region. In the outer national inversion, the average CH_4 emissions increased by 5.1%, while in the inner nested inversion, the increase was 4.3%. This highlights the necessity of expanding the inversion scope to mitigate the influence of boundary condition errors on the inversion of central regions.

Furthermore, by comparing the difference in CH_4 emissions over the inner domain between two outer national inversions with that between two inner nested regional inversions (BASE and SENS), we found that the two inner regional inversions exhibited a 23.1% smaller discrepancy. This indicates that adopting a nested inversion approach is essential, which can further reduce boundary errors during inner inversion through outer optimization, thereby enhancing the robustness of the inversion process.

https://doi.org/10.5194/egusphere-2025-2669
Preprint. Discussion started: 7 July 2025

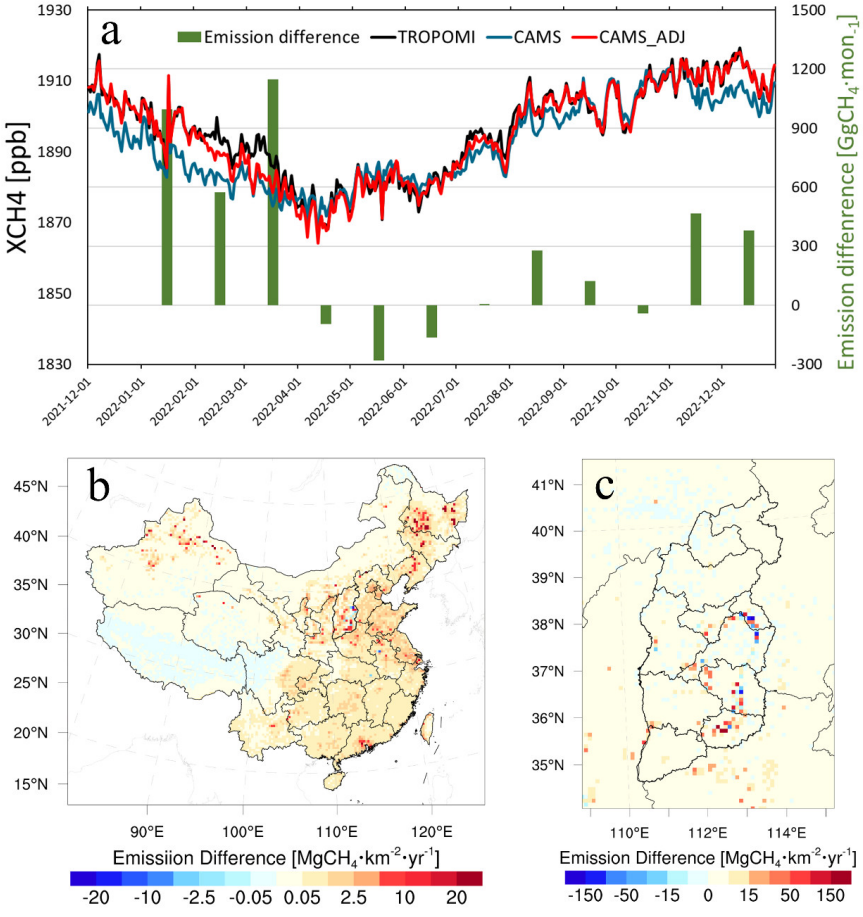

589

590 **Figure 7** Differences in XCH_4 column concentrations (ppb) between TROPOMI-adjusted and
591 unadjusted CAMS fields, along with the induced monthly posterior CH_4 emission differences (SENS
592 - BASE) over China (a); differences in two posterior emissions ($MgCH_4 \cdot km^{-2} \cdot yr^{-1}$) derived from
593 unadjusted and adjusted boundaries over China (b) and Shanxi Province (c)

594 Our inversion results are generally lower than previous emission estimates. By comparing the
595 differences in emissions from the inner region at different resolutions, we found that in both the BASE
596 and SENS experiments, emissions inverted in the inner region (9 km) were typically 7.6% and 8.4%
597 lower than those in the outer region (27 km), respectively. This discrepancy likely arises because
598 higher-resolution simulations excel at capturing localized emission hotspots that lead to elevated
599 concentration values. Therefore, compared to other coarse-resolution inversions, this study tends to

https://doi.org/10.5194/egusphere-2025-2669
Preprint. Discussion started: 7 July 2025

adjust emissions downward to better align with observations. Additionally, China's 2022 COVID-19 restrictions, the most stringent since 2020, may be another factor driving lower emissions due to production shutdowns and home quarantine. Peng et al. (2022) combined bottom-up and top-down approaches to quantify CH_4 source changes, revealing a 1.2 $Tg{\cdot}CH_4\,yr^{-1}$ reduction in anthropogenic CH_4 emissions in 2020 compared to 2019. Taking oil and gas sector as an example, an IEA report stated that global CH_4 emissions from oil and gas operations decreased by approximately 10% year-on-year in 2020 (IEA, 2021), primarily attributed to reduced oil and gas production during the pandemic (Thorpe et al., 2023).

5 Summary and conclusions

In this study, we developed a Regional Methane Assimilation System (RegGCAS-CH_4) based on the WRF-CMAQ model and EnKF algorithm to perform high-resolution nested inversions of China's CH_4 emissions using TROPOMI XCH_4 retrievals. Taking the EDGAR v8 as prior emissions, the daily anthropogenic CH_4 emissions over China in 2022 were inferred.

Using TROPOMI XCH_4 as constraints, we revealed significant overestimations in the prior emissions. Nationally, the posterior anthropogenic CH_4 emissions in 2022 were estimated to be 45.1 $TgCH_4{\cdot}yr^{-1}$, 36.5% lower than the EDGAR inventory, mainly driven by the decreases in the coal and waste sectors. North China experienced the most substantial reduction, with a 56.9% decrease, mainly due to downward revisions in the coal and enteric fermentation sectors. In Shanxi Province, influenced by dominant sources of coal mining, the posterior emissions decreased by 46.3% compared to the EDGAR inventory, with value of 4.8 $TgCH_4{\cdot}yr^{-1}$. The monthly variation of posterior emissions showed a pattern of being low in winter and high in summer. Except for the rice cultivation and waste sectors, which showed some increases in certain months related to seasonal growth stages and temperature-driven methanogen activity, respectively, other sectors exhibited varying degrees of reduction. Observation-constrained emissions significantly improved the performance of simulations regarding XCH_4 columns, as well as surface CH_4 in both the entire region and Shanxi Province, reducing biases by 46.0%, 58.6%, and 96.0%, respectively. This highlights the effectiveness of RegGCAS-CH_4 in reducing uncertainty in CH_4 emissions. Sensitivity inversions highlight the importance of high-resolution satellite-based nested inversions in accurately estimating CH_4 emissions, especially in reducing the impact of boundary condition errors on emission inversions.

https://doi.org/10.5194/egusphere-2025-2669
Preprint. Discussion started: 7 July 2025

Top-down inversions usually result in lower emissions compared to those constructed by bottom-up methods. When comparing our posterior emissions with other inventories, our estimates were the lowest among both bottom-up and top-down estimations. On average, they were 22.0% lower than bottom-up inventories and 16.6% lower than previous top-down estimates. The high-resolution simulations employed in this study are capable of more accurately simulating local high concentration values, and thus, the reduction in emissions is greater than that in previous studies. The overestimation of China's CH_4 emissions may have led to an overestimation of the country's climate change mitigation burden. The more accurate emission estimates presented here not only enhance our understanding of the CH_4 budget but also contribute to more effective global climate change mitigation efforts.

Data availability

The TROPOMI XCH_4 data is publicly available for download at the Copernicus Data Space Ecosystem (https://browser.dataspace.copernicus.eu/, last access: August 5, 2024). The observations used for evaluation and the posterior emissions and simulations produced in this study can be accessed at https://doi.org/10.5281/zenodo.15602944 (Feng, 2025).

Author contribution

SF, FJ and YZ conceived and designed the research. SF developed the RegGCAS-CH_4 system, analyzed data, and prepared the paper. SW evaluated the CH_4 simulation in Shanxi Province. HC, HZ, SB, HW, and WJ reviewed and commented on the paper.

Competing interests

At least one of the (co-)authors is a member of the editorial board of Atmospheric Chemistry and Physics.

Acknowledgements

This work is supported by the National Key R&D Program of China (Grant No: 2022YFE0209100), the National Natural Science Foundation of China (Grant Nos. 42305116 and U24A20590), the

https://doi.org/10.5194/egusphere-2025-2669
Preprint. Discussion started: 7 July 2025

Natural Science Foundation of Jiangsu Province of China (Grant No. BK20230801), and the Shanxi Provincial Basic Research Program Joint Funding Project (Meteorology) (Grant No. 202403011232002). We thank Professor Euan G. Nisbet for his valuable feedback and constructive comments that enhanced the clarity and quality of this paper. We also gratefully acknowledge the High-Performance Computing Center (HPCC) of Nanjing University for supporting the numerical calculations in this paper on its blade cluster system.

References

Agustí-Panareda, A., Barré, J., Massart, S., Inness, A., Aben, I., Ades, M., Baier, B. C., Balsamo, G., Borsdorff, T., Bousserez, N., Boussetta, S., Buchwitz, M., Cantarello, L., Crevoisier, C., Engelen, R., Eskes, H., Flemming, J., Garrigues, S., Hasekamp, O., Huijnen, V., Jones, L., Kipling, Z., Langerock, B., McNorton, J., Meilhac, N., Noël, S., Parrington, M., Peuch, V. H., Ramonet, M., Razinger, M., Reuter, M., Ribas, R., Suttie, M., Sweeney, C., Tarniewicz, J., and Wu, L.: Technical note: The CAMS greenhouse gas reanalysis from 2003 to 2020, Atmos. Chem. Phys., 23, 3829-3859, 10.5194/acp-23-3829-2023, 2023.

Alexe, M., Bergamaschi, P., Segers, A., Detmers, R., Butz, A., Hasekamp, O., Guerlet, S., Parker, R., Boesch, H., Frankenberg, C., Scheepmaker, R. A., Dlugokencky, E., Sweeney, C., Wofsy, S. C., and Kort, E. A.: Inverse modelling of CH_4 emissions for 2010–2011 using different satellite retrieval products from GOSAT and SCIAMACHY, Atmos. Chem. Phys., 15, 113-133, 10.5194/acp-15-113-2015, 2015.

Bai, S., Zhang, Y., Li, F., Yan, Y., Chen, H., Feng, S., Jiang, F., Sun, S., Wang, Z., Zhou, C., Zhou, W., and Zhao, S.: High-resolution satellite estimates of coal mine methane emissions from local to regional scales in Shanxi, China, Science of The Total Environment, 950, 175446, 10.1016/j.scitotenv.2024.175446, 2024.

Bergamaschi, P., Houweling, S., Segers, A., Krol, M., Frankenberg, C., Scheepmaker, R. A., Dlugokencky, E., Wofsy, S. C., Kort, E. A., Sweeney, C., Schuck, T., Brenninkmeijer, C., Chen, H., Beck, V., and Gerbig, C.: Atmospheric CH_4 in the first decade of the 21st century: Inverse modeling analysis using SCIAMACHY satellite retrievals and NOAA surface measurements, Journal of Geophysical Research: Atmospheres, 118, 7350-7369, 10.1002/jgrd.50480, 2013.

Bloom, A. A., Bowman, K. W., Lee, M., Turner, A. J., Schroeder, R., Worden, J. R., Weidner, R. J., McDonald, K. C., and Jacob, D. J.: CMS: Global 0.5-deg Wetland Methane Emissions and

https://doi.org/10.5194/egusphere-2025-2669
Preprint. Discussion started: 7 July 2025

Uncertainty (WetCHARTs v1.3.1), in, ORNL Distributed Active Archive Center, 2021.

Bruhwiler, L., Dlugokencky, E., Masarie, K., Ishizawa, M., Andrews, A., Miller, J., Sweeney, C., Tans, P., and Worthy, D.: CarbonTracker-CH_4: an assimilation system for estimating emissions of atmospheric methane, Atmos. Chem. Phys., 14, 8269-8293, 10.5194/acp-14-8269-2014, 2014.

Byun, D., and Schere, K. L.: Review of the governing equations, computational algorithms, and other components of the models-3 Community Multiscale Air Quality (CMAQ) modeling system, Applied Mechanics Reviews, 59, 51-77, 10.1115/1.2128636, 2006.

Chen, Z., Jacob, D. J., Nesser, H., Sulprizio, M. P., Lorente, A., Varon, D. J., Lu, X., Shen, L., Qu, Z., Penn, E., and Yu, X.: Methane emissions from China: a high-resolution inversion of TROPOMI satellite observations, Atmos. Chem. Phys., 22, 10809-10826, 10.5194/acp-22-10809-2022, 2022.

Evensen, G.: Sequential data assimilation with a nonlinear quasi-geostrophic model using Monte Carlo methods to forecast error statistics, Journal Of Geophysical Research-Oceans, 99, 10143-10162, 10.1029/94jc00572, 1994.

Feng, S.: CO Emissions Inferred From Surface CO Observations Over China in December 2013 and 2017, Journal of Geophysical Research-Atmospheres, 125, 10.1029/2019jd031808, 2020.

Feng, S.: Anthropogenic CH_4 Emissions over China in 2022 Inverted Using TROPOMI XCH4 Retrievals [Data set]. Zenodo. 10.5281/zenodo.15602944, 2025.

Feng, S., Jiang, F., Wu, Z., Wang, H., Ju, W., and Wang, H.: CO Emissions Inferred From Surface CO Observations Over China in December 2013 and 2017, Journal of Geophysical Research-Atmospheres, 125, 10.1029/2019jd031808, 2020.

Feng, S., Jiang, F., Wang, H., Shen, Y., Zheng, Y., Zhang, L., Lou, C., and Ju, W.: Anthropogenic emissions estimated using surface observations and their impacts on PM2.5 source apportionment over the Yangtze River Delta, China, Science of The Total Environment, 828, 154522, 10.1016/j.scitotenv.2022.154522, 2022.

Feng, S., Jiang, F., Wu, Z., Wang, H., He, W., Shen, Y., Zhang, L., Zheng, Y., Lou, C., Jiang, Z., and Ju, W.: A Regional multi-Air Pollutant Assimilation System (RAPAS v1.0) for emission estimates: system development and application, Geosci. Model Dev., 16, 5949-5977, 10.5194/gmd-16-5949-2023, 2023.

Feng, S., Jiang, F., Wang, H., Liu, Y., He, W., Wang, H., Shen, Y., Zhang, L., Jia, M., Ju, W., and Chen, J. M.: China's Fossil Fuel CO_2 Emissions Estimated Using Surface Observations of Coemitted NO2, Environmental Science & Technology, 58, 8299-8312, 10.1021/acs.est.3c07756, 2024.

https://doi.org/10.5194/egusphere-2025-2669
Preprint. Discussion started: 7 July 2025

719 Gao, J., Guan, C., and Zhang, B.: China's CH_4 emissions from coal mining: A review of current bottom-
720 up inventories, Science of The Total Environment, 725, 138295, 10.1016/j.scitotenv.2020.138295,
721 2020.

722 Gao, J., Guan, C., Zhang, B., and Li, K.: Decreasing methane emissions from China's coal mining with
723 rebounded coal production, Environmental Research Letters, 16, 124037, 10.1088/1748-
724 9326/ac38d8, 2021.

725 Gaspari, G., and Cohn, S. E.: Construction of correlation functions in two and three dimensions,
726 Quarterly Journal of the Royal Meteorological Society, 125, 723-757, 10.1256/smsqj.55416, 1999.

727 GMP: Global methane Pledge, https://www.globalmethanepledge.org/resources/global-methane-
728 pledge, last access: 12 Febrary 2025, 2023.

729 Hoesly, R. M., Smith, S. J., Feng, L., Klimont, Z., Janssens-Maenhout, G., Pitkanen, T., Seibert, J. J.,
730 Vu, L., Andres, R. J., Bolt, R. M., Bond, T. C., Dawidowski, L., Kholod, N., Kurokawa, J. I., Li,
731 M., Liu, L., Lu, Z., Moura, M. C. P., O'Rourke, P. R., and Zhang, Q.: Historical (1750–2014)
732 anthropogenic emissions of reactive gases and aerosols from the Community Emissions Data
733 System (CEDS), Geosci. Model Dev., 11, 369-408, 10.5194/gmd-11-369-2018, 2018.

734 Houtekamer, P. L., and Mitchell, H. L.: A sequential ensemble Kalman filter for atmospheric data
735 assimilation, Monthly Weather Review, 129, 123-137, 10.1175/1520-
736 0493(2001)129<0123:asekff>2.0.co;2, 2001.

737 Hu, C., Zhang, J., Qi, B., Du, R., Xu, X., Xiong, H., Liu, H., Ai, X., Peng, Y., and Xiao, W.: Global
738 warming will largely increase waste treatment CH_4 emissions in Chinese megacities: insight from
739 the first city-scale CH_4 concentration observation network in Hangzhou, China, Atmos. Chem.
740 Phys., 23, 4501-4520, 10.5194/acp-23-4501-2023, 2023.

741 IEA: Methane Tracker 2021, https://www.iea.org/reports/methane-tracker-2021, last access: 5 April
742 2025, 2021.

743 Jamali, H., Livesley, S. J., Dawes, T. Z., Cook, G. D., Hutley, L. B., and Arndt, S. K.: Diurnal and
744 seasonal variations in CH_4 flux from termite mounds in tropical savannas of the Northern Territory,
745 Australia, Agricultural and Forest Meteorology, 151, 1471-1479,
746 10.1016/j.agrformet.2010.06.009, 2011.

747 Janssens-Maenhout, G., Crippa, M., Guizzardi, D., Muntean, M., Schaaf, E., Dentener, F.,
748 Bergamaschi, P., Pagliari, V., Olivier, J. G. J., Peters, J. A. H. W., van Aardenne, J. A., Monni, S.,
749 Doering, U., Petrescu, A. M. R., Solazzo, E., and Oreggioni, G. D.: EDGAR v4.3.2 Global Atlas
750 of the three major greenhouse gas emissions for the period 1970–2012, Earth Syst. Sci. Data, 11,

https://doi.org/10.5194/egusphere-2025-2669
Preprint. Discussion started: 7 July 2025

959-1002, 10.5194/essd-11-959-2019, 2019.

Jiang, F., Wang, H., Chen, J. M., Ju, W., Tian, X., Feng, S., Li, G., Chen, Z., Zhang, S., Lu, X., Liu, J., Wang, H., Wang, J., He, W., and Wu, M.: Regional CO_2 fluxes from 2010 to 2015 inferred from GOSAT XCO_2 retrievals using a new version of the Global Carbon Assimilation System, Atmos. Chem. Phys., 21, 1963-1985, 10.5194/acp-21-1963-2021, 2021.

Kou, X., Peng, Z., Han, X., Li, J., Qin, L., Zhang, M., Parker, R. J., and Boesch, H.: China's methane emissions derived from the inversion of GOSAT observations with a CMAQ and EnKS-based regional data assimilation system, Atmospheric Pollution Research, 16, 102333, 10.1016/j.apr.2024.102333, 2025.

Liang, R., Zhang, Y., Chen, W., Zhang, P., Liu, J., Chen, C., Mao, H., Shen, G., Qu, Z., Chen, Z., Zhou, M., Wang, P., Parker, R. J., Boesch, H., Lorente, A., Maasakkers, J. D., and Aben, I.: East Asian methane emissions inferred from high-resolution inversions of GOSAT and TROPOMI observations: a comparative and evaluative analysis, Atmos. Chem. Phys., 23, 8039-8057, 10.5194/acp-23-8039-2023, 2023.

Lin, X., Zhang, W., Crippa, M., Peng, S., Han, P., Zeng, N., Yu, L., and Wang, G.: A comparative study of anthropogenic CH_4 emissions over China based on the ensembles of bottom-up inventories, Earth Syst. Sci. Data, 13, 1073-1088, 10.5194/essd-13-1073-2021, 2021.

Liu, G., Peng, S., Lin, X., Ciais, P., Li, X., Xi, Y., Lu, Z., Chang, J., Saunois, M., Wu, Y., Patra, P., Chandra, N., Zeng, H., and Piao, S.: Recent Slowdown of Anthropogenic Methane Emissions in China Driven by Stabilized Coal Production, Environmental Science & Technology Letters, 8, 739-746, 10.1021/acs.estlett.1c00463, 2021.

Lorente, A., Borsdorff, T., Martinez-Velarte, M. C., Butz, A., Hasekamp, O. P., Wu, L., and Landgraf, J.: Evaluation of the methane full-physics retrieval applied to TROPOMI ocean sun glint measurements, Atmos. Meas. Tech., 15, 6585-6603, 10.5194/amt-15-6585-2022, 2022.

Lu, X., Jacob, D. J., Zhang, Y., Shen, L., Sulprizio, M. P., Maasakkers, J. D., Varon, D. J., Qu, Z., Chen, Z., Hmiel, B., Parker, R. J., Boesch, H., Wang, H., He, C., and Fan, S.: Observation-derived 2010-2019 trends in methane emissions and intensities from US oil and gas fields tied to activity metrics, Proceedings of the National Academy of Sciences, 120, e2217900120, doi:10.1073/pnas.2217900120, 2023.

Lu, Y. Y., Zhang, H. D., Zhou, Z., Ge, Z. L., Chen, C. J., Hou, Y. D., and Ye, M. L.: Current Status and Effective Suggestions for Efficient Exploitation of Coalbed Methane in China: A Review, Energy & Fuels, 35, 9102-9123, 10.1021/acs.energyfuels.1c00460, 2021.

https://doi.org/10.5194/egusphere-2025-2669
Preprint. Discussion started: 7 July 2025

Maasakkers, J. D., Jacob, D. J., Sulprizio, M. P., Scarpelli, T. R., Nesser, H., Sheng, J. X., Zhang, Y., Hersher, M., Bloom, A. A., Bowman, K. W., Worden, J. R., Janssens-Maenhout, G., and Parker, R. J.: Global distribution of methane emissions, emission trends, and OH concentrations and trends inferred from an inversion of GOSAT satellite data for 2010–2015, Atmos. Chem. Phys., 19, 7859-7881, 10.5194/acp-19-7859-2019, 2019.

MECAP: Methane Emission Control Action Plan, https://www.mee.gov.cn/xxgk2018/xxgk/xxgk03/202311/t20231107_1055437.html, last access: 12 May 2025, 2023.

Miller, S. M., Michalak, A. M., Detmers, R. G., Hasekamp, O. P., Bruhwiler, L. M. P., and Schwietzke, S.: China's coal mine methane regulations have not curbed growing emissions, Nature Communications, 10, 303, 10.1038/s41467-018-07891-7, 2019.

Miyazaki, K., Eskes, H., Sudo, K., Boersma, K. F., Bowman, K., and Kanaya, Y.: Decadal changes in global surface NOx emissions from multi-constituent satellite data assimilation, Atmospheric Chemistry and Physics, 17, 807-837, 10.5194/acp-17-807-2017, 2017.

Murguia-Flores, F., Arndt, S., Ganesan, A. L., Murray-Tortarolo, G., and Hornibrook, E. R. C.: Soil Methanotrophy Model (MeMo v1.0): a process-based model to quantify global uptake of atmospheric methane by soil, Geosci. Model Dev., 11, 2009-2032, 10.5194/gmd-11-2009-2018, 2018.

Nesser, H., Jacob, D. J., Maasakkers, J. D., Lorente, A., Chen, Z., Lu, X., Shen, L., Qu, Z., Sulprizio, M. P., Winter, M., Ma, S., Bloom, A. A., Worden, J. R., Stavins, R. N., and Randles, C. A.: High-resolution US methane emissions inferred from an inversion of 2019 TROPOMI satellite data: contributions from individual states, urban areas, and landfills, Atmos. Chem. Phys., 24, 5069-5091, 10.5194/acp-24-5069-2024, 2024.

Nisbet, E. G.: New hope for methane reduction, Science, 382, 1093-1093, doi:10.1126/science.adn0134, 2023.

Oh, Y., Bruhwiler, L., Lan, X., Basu, S., Schuldt, K., Thoning, K., Michel, S. E., Clark, R., Miller, J. B., Andrews, A., Sherwood, O., Etiope, G., Crippa, M., Liu, L., Zhuang, Q., Randerson, J., van der Werf, G., Aalto, T., Amendola, S., Andra, S. C., Andrade, M., Nguyen, N. A., Aoki, S., Apadula, F., Arifin, I. B., Arnold, S., Arshinov, M., Baier, B., Bergamaschi, P., Biermann, T., Biraud, S. C., Blanc, P.-E., Brailsford, G., Chen, H., Colomb, A., Couret, C., Cristofanelli, P., Cuevas, E., Chmura, L., Delmotte, M., Emmenegger, L., Esenzhanova, G., Fujita, R., Gatti, L., Guerette, E.-A., Haszpra, L., Heliasz, M., Hermansen, O., Holst, J., Di Iorio, T., Jordan, A., Jennifer, M.-W., Karion, A., Kawasaki, T., Kazan, V., Keronen, P., Kim, S.-Y., Kneuer, T.,

https://doi.org/10.5194/egusphere-2025-2669
Preprint. Discussion started: 7 July 2025

Kominkova, K., Kozlova, E., Krummel, P., Kubistin, D., Labuschagne, C., Langenfelds, R., Laurent, O., Laurila, T., Lee, H., Lehner, I., Leuenberger, M., Lindauer, M., Lopez, M., Mahdi, R., Mammarella, I., Manca, G., Marek, M. V., Mazière, M. D., McKain, K., Meinhardt, F., Miller, C. E., Mölder, M., Moncrieff, J., Moosen, H., Moreno, C., Morimoto, S., Myhre, C. L., Nahas, A. C., Necki, J., Nichol, S., O'Doherty, S., Paramonova, N., Piacentino, S., Pichon, J. M., Plass-Dülmer, C., Ramonet, M., Ries, L., di Sarra, A. G., Sasakawa, M., Say, D., Schaefer, H., Scheeren, B., Schmidt, M., Schumacher, M., Sha, M. K., Shepson, P., Smale, D., Smith, P. D., Steinbacher, M., Sweeney, C., Takatsuji, S., Torres, G., Tørseth, K., Trisolino, P., Turnbull, J., Uhse, K., Umezawa, T., Vermeulen, A., Vimont, I., Vitkova, G., Wang, H.-J., Worthy, D., and Xueref-Remy, I.: CarbonTracker CH_4 2023, NOAA Global Monitoring Laboratory, 2023.

Pandey, S., Houweling, S., Krol, M., Aben, I., Chevallier, F., Dlugokencky, E. J., Gatti, L. V., Gloor, E., Miller, J. B., Detmers, R., Machida, T., and Röckmann, T.: Inverse modeling of GOSAT-retrieved ratios of total column CH_4 and CO_2 for 2009 and 2010, Atmos. Chem. Phys., 16, 5043-5062, 10.5194/acp-16-5043-2016, 2016.

Pandey, S., Gautam, R., Houweling, S., van der Gon, H. D., Sadavarte, P., Borsdorff, T., Hasekamp, O., Landgraf, J., Tol, P., van Kempen, T., Hoogeveen, R., van Hees, R., Hamburg, S. P., Maasakkers, J. D., and Aben, I.: Satellite observations reveal extreme methane leakage from a natural gas well blowout, Proceedings of the National Academy of Sciences, 116, 26376-26381, doi:10.1073/pnas.1908712116, 2019.

Peng, S., Lin, X., Thompson, R. L., Xi, Y., Liu, G., Hauglustaine, D., Lan, X., Poulter, B., Ramonet, M., Saunois, M., Yin, Y., Zhang, Z., Zheng, B., and Ciais, P.: Wetland emission and atmospheric sink changes explain methane growth in 2020, Nature, 612, 477-482, 10.1038/s41586-022-05447-w, 2022.

Peng, S., Giron, C., Liu, G., d'Aspremont, A., Benoit, A., Lauvaux, T., Lin, X., de Almeida Rodrigues, H., Saunois, M., and Ciais, P.: High-resolution assessment of coal mining methane emissions by satellite in Shanxi, China, iScience, 26, 108375, 10.1016/j.isci.2023.108375, 2023.

Prather, M. J.: Lifetimes and time scales in atmospheric chemistry, Philosophical Transactions of the Royal Society A: Mathematical, Physical and Engineering Sciences, 365, 1705-1726, doi:10.1098/rsta.2007.2040, 2007.

Qin, K., Hu, W., He, Q., Lu, F., and Cohen, J. B.: Individual coal mine methane emissions constrained by eddy covariance measurements: low bias and missing sources, Atmos. Chem. Phys., 24, 3009-3028, 10.5194/acp-24-3009-2024, 2024.

Qu, Z., Jacob, D. J., Shen, L., Lu, X., Zhang, Y., Scarpelli, T. R., Nesser, H., Sulprizio, M. P.,

https://doi.org/10.5194/egusphere-2025-2669
Preprint. Discussion started: 7 July 2025

Maasakkers, J. D., Bloom, A. A., Worden, J. R., Parker, R. J., and Delgado, A. L.: Global distribution of methane emissions: a comparative inverse analysis of observations from the TROPOMI and GOSAT satellite instruments, Atmos. Chem. Phys., 21, 14159-14175, 10.5194/acp-21-14159-2021, 2021.

Saunois, M., Martinez, A., Poulter, B., Zhang, Z., Raymond, P. A., Regnier, P., Canadell, J. G., Jackson, R. B., Patra, P. K., Bousquet, P., Ciais, P., Dlugokencky, E. J., Lan, X., Allen, G. H., Bastviken, D., Beerling, D. J., Belikov, D. A., Blake, D. R., Castaldi, S., Crippa, M., Deemer, B. R., Dennison, F., Etiope, G., Gedney, N., Höglund-Isaksson, L., Holgerson, M. A., Hopcroft, P. O., Hugelius, G., Ito, A., Jain, A. K., Janardanan, R., Johnson, M. S., Kleinen, T., Krummel, P. B., Lauerwald, R., Li, T., Liu, X., McDonald, K. C., Melton, J. R., Mühle, J., Müller, J., Murguia-Flores, F., Niwa, Y., Noce, S., Pan, S., Parker, R. J., Peng, C., Ramonet, M., Riley, W. J., Rocher-Ros, G., Rosentreter, J. A., Sasakawa, M., Segers, A., Smith, S. J., Stanley, E. H., Thanwerdas, J., Tian, H., Tsuruta, A., Tubiello, F. N., Weber, T. S., van der Werf, G. R., Worthy, D. E. J., Xi, Y., Yoshida, Y., Zhang, W., Zheng, B., Zhu, Q., Zhu, Q., and Zhuang, Q.: Global Methane Budget 2000–2020, Earth Syst. Sci. Data, 17, 1873-1958, 10.5194/essd-17-1873-2025, 2025.

Scarpelli, T. R., Jacob, D. J., Grossman, S., Lu, X., Qu, Z., Sulprizio, M. P., Zhang, Y., Reuland, F., Gordon, D., and Worden, J. R.: Updated Global Fuel Exploitation Inventory (GFEI) for methane emissions from the oil, gas, and coal sectors: evaluation with inversions of atmospheric methane observations, Atmos. Chem. Phys., 22, 3235-3249, 10.5194/acp-22-3235-2022, 2022.

Schneising, O., Buchwitz, M., Hachmeister, J., Vanselow, S., Reuter, M., Buschmann, M., Bovensmann, H., and Burrows, J. P.: Advances in retrieving XCH_4 and XCO from Sentinel-5 Precursor: improvements in the scientific TROPOMI/WFMD algorithm, Atmos. Meas. Tech., 16, 669-694, 10.5194/amt-16-669-2023, 2023.

Schuldt, K. N., Mund, J., Aalto, T., Arlyn, A., Apadula, F., Jgor, A., Arnold, S., Baier, B., Bäni, L., Bartyzel, J., Bergamaschi, P., Biermann, T., Biraud, S. C., Pierre-Eric, B., Boenisch, H., Brailsford, G., Brand, W. A., Brunner, D., Bui, T. P. V., Van Den Bulk, P., Francescopiero, C., Chang, C. S., Huilin, C., Lukasz, C., St. Clair, J. M., Sites, C., Coletta, J. D., Colomb, A., Condori, L., Conen, F., Conil, S., Couret, C., Cristofanelli, P., Cuevas, E., Curcoll, R., Daube, B., Davis, K. J., Dean-Day, J. M., Delmotte, M., Ankur, D., DiGangi, E., DiGangi, J. P., Van Dinther, D., Elkins, J. W., Elsasser, M., Emmenegger, L., Fischer, M. L., Forster, G., Frumau, A., Fuente-Lastra, M., Galkowski, M., Gatti, L. V., Gehrlein, T., Gerbig, C., Francois, G., Gloor, E., Goto, D., Hammer, S., Hanisco, T. F., Haszpra, L., Hatakka, J., Heimann, M., Heimann, M., Heliasz, M., Heltai, D., Henne, S., Hensen, A., Hermans, C., Hermansen, O., Hintsa, E., Hoheisel, A., Holst, J., Di Iorio, T., Iraci, L. T., Ivakhov, V., Jaffe, D. A., Jordan, A., Joubert, W., Kang, H.-Y., Karion, A., Kazan,

https://doi.org/10.5194/egusphere-2025-2669
Preprint. Discussion started: 7 July 2025

V., Keeling, R. F., Keronen, P., Kers, B., Jooil, K., Klausen, J., Kneuer, T., Ko, M.-Y., Kolari, P., Kominkova, K., Kort, E., Kozlova, E., Krummel, P. B., Kubistin, D., Kulawik, S. S., Kumps, N., Labuschagne, C., Lan, X., Langenfelds, R. L., Lanza, A., Laurent, O., Laurila, T., Lauvaux, T., Lavric, J., Choong-Hoon, L., Haeyoung, L., Lee, J., Lehner, I., Lehtinen, K., Leppert, R., Leskinen, A., Leuenberger, M., Levin, I., Levula, J., Lindauer, M., Lindroth, A., Mikaell Ottosson, L., Loh, Z. M., Lopez, M., Lowry, D., Lunder, C. R., Machida, T., Mammarella, I., Manca, G., Manning, A., Marek, M. V., Marklund, P., Marrero, J. E., Martin, D., Martin, M. Y., Giordane, A. M., Matsueda, H., De Mazière, M., McKain, K., Meinhardt, F., Menoud, M., Jean-Marc, M., Miles, N. L., Miller, C. E., Miller, J. B., Mölder, M., Monteiro, V., Montzka, S., Moore, F., Moossen, H., Morgan, E., Josep-Anton, M., Morimoto, S., Müller-Williams, J., Munro, D., Mutuku, M., Myhre, C. L., Jaroslaw, N., Nichol, S., Nisbet, E., Niwa, Y., Njiru, D. M., Noe, S. M., O'Doherty, S., Obersteiner, F., Parworth, C. L., Peltola, O., Peters, W., Philippon, C., Piacentino, S., Pichon, J. M., Pickers, P., Pitt, J., Pittman, J., Plass-Dülmer, C., Platt, S. M., Popa, M. E., Prinzivalli, S., Ramonet, M., Richardson, S. J., Louis-Jeremy, R., Rivas, P. P., Röckmann, T., Rothe, M., Yves-Alain, R., Ju-Mee, R., Santoni, G., Di Sarra, A. G., Sasakawa, M., Scheeren, B., Schmidt, M., Schuck, T., Schumacher, M., Seifert, T., Sha, M. K., Shepson, P., Sloop, C. D., Smith, P. D., Sørensen, L. L., De Souza, R. A. F., Spain, G., Steger, D., Steinbacher, M., Stephens, B., Sweeney, C., Taipale, R., Takatsuji, S., Thoning, K., Timas, H., Torn, M., Trisolino, P., Turnbull, J., Van Der Veen, C., Vermeulen, A., Vimont, I., Viner, B., Vitkova, G., De Vries, M., Watson, A., Weiss, R., Weyrauch, D., Wofsy, S. C., Worsey, J., Worthy, D., Xueref-Remy, I., Yates, E. L., Dickon, Y., Yver-Kwok, C., Zaehle, S., Zahn, A., Zazzeri, G., Zellweger, C., and Miroslaw, Z.: Multi-laboratory compilation of atmospheric carbon dioxide data for the period 1983-2022; obspack_ch4_1_GLOBALVIEWplus_v6.0_2023-12-01, in, NOAA Global Monitoring Laboratory, 2023.

Sheng, J., Song, S., Zhang, Y., Prinn, R. G., and Janssens-Maenhout, G.: Bottom-Up Estimates of Coal Mine Methane Emissions in China: A Gridded Inventory, Emission Factors, and Trends, Environmental Science & Technology Letters, 6, 473-478, 10.1021/acs.estlett.9b00294, 2019.

Sheng, J., Tunnicliffe, R., Ganesan, A. L., Maasakkers, J. D., Shen, L., Prinn, R. G., Song, S., Zhang, Y., Scarpelli, T., Anthony Bloom, A., Rigby, M., Manning, A. J., Parker, R. J., Boesch, H., Lan, X., Zhang, B., Zhuang, M., and Lu, X.: Sustained methane emissions from China after 2012 despite declining coal production and rice-cultivated area, Environmental Research Letters, 16, 104018, 10.1088/1748-9326/ac24d1, 2021.

Shi, X., Peng, Y., Wang, S., Zhang, Y., Zhang, J., Song, H., Cui, Y., Sun, F., Liu, H., Xiao, Q., Hu, N., Xiao, W., Griffis, T. J., and Hu, C.: Revising the coal mining CH_4 emission factor based on

https://doi.org/10.5194/egusphere-2025-2669
Preprint. Discussion started: 7 July 2025

multiple inventories and atmospheric inversion approach at one of the world's largest coal production areas: Shanxi province, China, Science of The Total Environment, 965, 178616, 10.1016/j.scitotenv.2025.178616, 2025.

Skamarock, W. C., and Klemp, J. B.: A time-split nonhydrostatic atmospheric model for weather research and forecasting applications, Journal Of Computational Physics, 227, 3465-3485, 10.1016/j.jcp.2007.01.037, 2008.

Soulie, A., Granier, C., Darras, S., Zilbermann, N., Doumbia, T., Guevara, M., Jalkanen, J. P., Keita, S., Liousse, C., Crippa, M., Guizzardi, D., Hoesly, R., and Smith, S. J.: Global anthropogenic emissions (CAMS-GLOB-ANT) for the Copernicus Atmosphere Monitoring Service simulations of air quality forecasts and reanalyses, Earth Syst. Sci. Data, 16, 2261-2279, 10.5194/essd-16-2261-2024, 2024.

Stavert, A. R., Saunois, M., Canadell, J. G., Poulter, B., Jackson, R. B., Regnier, P., Lauerwald, R., Raymond, P. A., Allen, G. H., Patra, P. K., Bergamaschi, P., Bousquet, P., Chandra, N., Ciais, P., Gustafson, A., Ishizawa, M., Ito, A., Kleinen, T., Maksyutov, S., McNorton, J., Melton, J. R., Müller, J., Niwa, Y., Peng, S., Riley, W. J., Segers, A., Tian, H., Tsuruta, A., Yin, Y., Zhang, Z., Zheng, B., and Zhuang, Q.: Regional trends and drivers of the global methane budget, Global Change Biology, 28, 182-200, 10.1111/gcb.15901, 2022.

Steiner, M., Peters, W., Luijkx, I., Henne, S., Chen, H., Hammer, S., and Brunner, D.: European CH_4 inversions with ICON-ART coupled to the CarbonTracker Data Assimilation Shell, Atmos. Chem. Phys., 24, 2759-2782, 10.5194/acp-24-2759-2024, 2024.

Stohl, A., Aamaas, B., Amann, M., Baker, L. H., Bellouin, N., Berntsen, T. K., Boucher, O., Cherian, R., Collins, W., Daskalakis, N., Dusinska, M., Eckhardt, S., Fuglestvedt, J. S., Harju, M., Heyes, C., Hodnebrog, Ø., Hao, J., Im, U., Kanakidou, M., Klimont, Z., Kupiainen, K., Law, K. S., Lund, M. T., Maas, R., MacIntosh, C. R., Myhre, G., Myriokefalitakis, S., Olivié, D., Quaas, J., Quennehen, B., Raut, J. C., Rumbold, S. T., Samset, B. H., Schulz, M., Seland, Ø., Shine, K. P., Skeie, R. B., Wang, S., Yttri, K. E., and Zhu, T.: Evaluating the climate and air quality impacts of short-lived pollutants, Atmos. Chem. Phys., 15, 10529-10566, 10.5194/acp-15-10529-2015, 2015.

Thanwerdas, J., Saunois, M., Berchet, A., Pison, I., Vaughn, B. H., Michel, S. E., and Bousquet, P.: Variational inverse modeling within the Community Inversion Framework v1.1 to assimilate $\delta 13C(CH_4)$ and CH_4: a case study with model LMDz-SACS, Geosci. Model Dev., 15, 4831-4851, 10.5194/gmd-15-4831-2022, 2022.

Thompson, R. L., Stohl, A., Zhou, L. X., Dlugokencky, E., Fukuyama, Y., Tohjima, Y., Kim, S.-Y., Lee, H., Nisbet, E. G., Fisher, R. E., Lowry, D., Weiss, R. F., Prinn, R. G., O'Doherty, S., Young, D.,

https://doi.org/10.5194/egusphere-2025-2669
Preprint. Discussion started: 7 July 2025

and White, J. W. C.: Methane emissions in East Asia for 2000–2011 estimated using an atmospheric Bayesian inversion, Journal of Geophysical Research: Atmospheres, 120, 4352-4369, 10.1002/2014JD022394, 2015.

Thorpe, A. K., Kort, E. A., Cusworth, D. H., Ayasse, A. K., Bue, B. D., Yadav, V., Thompson, D. R., Frankenberg, C., Herner, J., Falk, M., Green, R. O., Miller, C. E., and Duren, R. M.: Methane emissions decline from reduced oil, natural gas, and refinery production during COVID-19, Environmental Research Communications, 5, 021006, 10.1088/2515-7620/acb5e5, 2023.

Tsuruta, A., Aalto, T., Backman, L., Hakkarainen, J., van der Laan-Luijkx, I. T., Krol, M. C., Spahni, R., Houweling, S., Laine, M., Dlugokencky, E., Gomez-Pelaez, A. J., van der Schoot, M., Langenfelds, R., Ellul, R., Arduini, J., Apadula, F., Gerbig, C., Feist, D. G., Kivi, R., Yoshida, Y., and Peters, W.: Global methane emission estimates for 2000–2012 from CarbonTracker Europe-CH_4 v1.0, Geosci. Model Dev., 10, 1261-1289, 10.5194/gmd-10-1261-2017, 2017.

Tu, Q., Hase, F., Qin, K., Cohen, J. B., Khosrawi, F., Zou, X., Schneider, M., and Lu, F.: Quantifying CH_4 emissions from coal mine aggregation areas in Shanxi, China, using TROPOMI observations and the wind-assigned anomaly method, Atmos. Chem. Phys., 24, 4875-4894, 10.5194/acp-24-4875-2024, 2024.

Turner, A. J., Jacob, D. J., Wecht, K. J., Maasakkers, J. D., Lundgren, E., Andrews, A. E., Biraud, S. C., Boesch, H., Bowman, K. W., Deutscher, N. M., Dubey, M. K., Griffith, D. W. T., Hase, F., Kuze, A., Notholt, J., Ohyama, H., Parker, R., Payne, V. H., Sussmann, R., Sweeney, C., Velazco, V. A., Warneke, T., Wennberg, P. O., and Wunch, D.: Estimating global and North American methane emissions with high spatial resolution using GOSAT satellite data, Atmos. Chem. Phys., 15, 7049-7069, 10.5194/acp-15-7049-2015, 2015.

van Wees, D., van der Werf, G. R., Randerson, J. T., Rogers, B. M., Chen, Y., Veraverbeke, S., Giglio, L., and Morton, D. C.: Global biomass burning fuel consumption and emissions at 500 m spatial resolution based on the Global Fire Emissions Database (GFED), Geosci. Model Dev., 15, 8411-8437, 10.5194/gmd-15-8411-2022, 2022.

Varon, D. J., Jacob, D. J., Sulprizio, M., Estrada, L. A., Downs, W. B., Shen, L., Hancock, S. E., Nesser, H., Qu, Z., Penn, E., Chen, Z., Lu, X., Lorente, A., Tewari, A., and Randles, C. A.: Integrated Methane Inversion (IMI 1.0): a user-friendly, cloud-based facility for inferring high-resolution methane emissions from TROPOMI satellite observations, Geosci. Model Dev., 15, 5787-5805, 10.5194/gmd-15-5787-2022, 2022.

Wang, F., Maksyutov, S., Tsuruta, A., Janardanan, R., Ito, A., Sasakawa, M., Machida, T., Morino, I., Yoshida, Y., Kaiser, J. W., Janssens-Maenhout, G., Dlugokencky, E. J., Mammarella, I., Lavric, J.

https://doi.org/10.5194/egusphere-2025-2669
Preprint. Discussion started: 7 July 2025

V., and Matsunaga, T.: Methane Emission Estimates by the Global High-Resolution Inverse Model Using National Inventories, Remote Sensing, 11, 2489, 10.3390/rs11212489, 2019.

Wang, Y., Zhang, Y., Tian, X., Wang, X., Yuan, W., Ding, J., Jiang, F., Jin, Z., Ju, W., Liang, R., Lu, X., Shen, L., Sun, S., Wang, T., Zhang, H., Zhao, M., and Piao, S.: Towards verifying and improving estimations of China's CO_2 and CH_4 budgets using atmospheric inversions, National Science Review, 12, 10.1093/nsr/nwaf090, 2025.

Whitaker, J. S., and Hamill, T. M.: Ensemble data assimilation without perturbed observations, Monthly Weather Review, 130, 1913-1924, 10.1175/1520-0493(2002)130<1913:Edawpo>2.0.Co;2, 2002.

Wunch, D., Toon, G. C., Blavier, J.-F. L., Washenfelder, R. A., Notholt, J., Connor, B. J., Griffith, D. W. T., Sherlock, V., and Wennberg, P. O.: The Total Carbon Column Observing Network, Philosophical Transactions of the Royal Society A: Mathematical, Physical and Engineering Sciences, 369, 2087-2112, doi:10.1098/rsta.2010.0240, 2011.

Zhang, X., Zhou, C., Zhang, Y., Lu, X., Xiao, X., Wang, F., Song, J., Guo, Y., Leung, K. K. M., Cao, J., and Gao, M.: Where to place methane monitoring sites in China to better assist carbon management, npj Climate and Atmospheric Science, 6, 32, 10.1038/s41612-023-00359-6, 2023.

Zhang, Y., Jacob, D. J., Lu, X., Maasakkers, J. D., Scarpelli, T. R., Sheng, J. X., Shen, L., Qu, Z., Sulprizio, M. P., Chang, J., Bloom, A. A., Ma, S., Worden, J., Parker, R. J., and Boesch, H.: Attribution of the accelerating increase in atmospheric methane during 2010–2018 by inverse analysis of GOSAT observations, Atmos. Chem. Phys., 21, 3643-3666, 10.5194/acp-21-3643-2021, 2021.

Zhang, Y., Fang, S., Chen, J., Lin, Y., Chen, Y., Liang, R., Jiang, K., Parker, R. J., Boesch, H., Steinbacher, M., Sheng, J.-X., Lu, X., Song, S., and Peng, S.: Observed changes in China's methane emissions linked to policy drivers, Proceedings of the National Academy of Sciences, 119, e2202742119, doi:10.1073/pnas.2202742119, 2022.

Zhang, Z., Feng, S., Chen, Y., Liu, Q., Ju, W., Xiao, W., Huang, C., Wang, Y., Wang, H., Jia, M., Wang, X., and Jiang, F.: Development of a regional carbon assimilation system and its application for estimating fossil fuel carbon emissions in the Yangtze River Delta, China, Science of The Total Environment, 957, 177720, 10.1016/j.scitotenv.2024.177720, 2024.

Zhao, M., Tian, X., Wang, Y., Wang, X., Ciais, P., Jin, Z., Zhang, H., Wang, T., Ding, J., and Piao, S.: Slowdown in China's methane emission growth, National Science Review, 11, 10.1093/nsr/nwae223, 2024.